A New Functional Form and New Fitting Techniques for Equations of State with Application to Pentafluoroethane (HFC-125)

Eric W. Lemmon[a)]

Physical and Chemical Properties Division, National Institute of Standards and Technology, 325 Broadway, Boulder, Colorado 80305

Richard T Jacobsen

Idaho National Engineering and Environmental Laboratory, P.O. Box 1625, Idaho Falls, Idaho 83415-2214

(Received 30 December 2003; revised manuscript received 25 June 2004; accepted 29 June 2004; published online 30 March 2005)

A widely used form of an equation of state explicit in Helmholtz energy has been modified with new terms to eliminate certain undesirable characteristics in the two phase region. Modern multiparameter equations of state exhibit behavior in the two phase that is inconsistent with the physical behavior of fluids. The new functional form overcomes this dilemma and results in equations of state for pure fluids that are more fundamentally consistent. With the addition of certain nonlinear fitting constraints, the new equation now achieves proper phase stability, i.e., only one solution exists for phase equilibrium at a given state. New fitting techniques have been implemented to ensure proper extrapolation of the equation at low temperatures, in the vapor phase at low densities, and at very high temperatures and pressures. A formulation is presented for the thermodynamic properties of refrigerant 125 (pentafluoroethane, CHF_2-CF_3) using the new terms and fitting techniques. The equation of state is valid for temperatures from the triple point temperature (172.52 K) to 500 K and for pressures up to 60 MPa. The formulation can be used for the calculation of all thermodynamic properties, including density, heat capacity, speed of sound, energy, and saturation properties. Comparisons to available experimental data are given that establish the accuracy of calculated properties. The estimated uncertainties of properties calculated using the new equation are 0.1% in density, 0.5% in heat capacities, 0.05% in the vapor phase speed of sound at pressures less than 1 MPa, 0.5% in the speed of sound elsewhere, and 0.1% in vapor pressure. Deviations in the critical region are higher for all properties except vapor pressure.
[DOI: 10.1063/1.1797813]

Key words: caloric properties; density; equation of state; fundamental equation; HFC-125; pentafluoroethane; R-125; thermodynamic properties.

Contents

[a)]Electronic mail: ericl@boulder.nist.gov

List of Tables

List of Figures

List of Symbols

Symbol	Physical quantity	Unit
a	Helmholtz energy	J/mol
B	Second virial coefficient	dm^3/mol
C	Third virial coefficient	$(dm^3/mol)^2$
c_p	Isobaric heat capacity	J/(mol·K)
c_v	Isochoric heat capacity	J/(mol·K)
c_σ	Saturation heat capacity	J/(mol·K)
d	Exponent on density	
D	Fourth virial coefficient	$(dm^3/mol)^3$
g	Gibbs energy	J/mol
h	Enthalpy	J/mol
l	Exponent on density	
m	Exponent on temperature	
M	Molar mass	g/mol
N	Coefficient	
p	Pressure	MPa
q	Quality	
R	Molar gas constant	J/(mol·K)
s	Entropy	J/(mol·K)
S	Sum of squares of deviations	
t	Exponent on temperature	
T	Temperature	K
u	Internal energy	J/mol
v	Molar volume	dm^3/mol
w	Speed of sound	m/s
W	Weight used in fitting	
Z	Compressibility factor $[Z=p/(\rho RT)]$	
α	Reduced Helmholtz energy $[\alpha=a/(RT)]$	
β	Critical exponent	
δ	Reduced density ($\delta=\rho/\rho_c$)	
ϕ	Fugacity coefficient	
ρ	Molar density	mol/dm^3
τ	Inverse reduced temperature ($\tau=T_c/T$)	

Superscripts

0	Ideal gas property
r	Residual
$'$	Saturated liquid state
$''$	Saturated vapor state

Subscripts

0	Reference state property
c	Critical point property
calc	Calculated using an equation
data	Experimental value
l	Liquid property
nbp	Normal boiling point property
tp	Triple point property
ν	Vapor property
σ	Saturation property

Physical Constants and Characteristic Properties of R-125

Symbol	Quantity	Value
R	Molar gas constant	8.314 472 J/(mol·K)
M	Molar mass	120.0214 g/mol
T_c	Critical temperature	339.173 K
p_c	Critical pressure	3.6177 MPa
ρ_c	Critical density	4.779 mol/dm^3
T_{tp}	Triple point temperature	172.52 K
p_{tp}	Triple point pressure	0.002 914 MPa
ρ_{tpv}	Vapor density at the triple point	0.002 038 mol/dm^3
ρ_{tpl}	Liquid density at the triple point	14.086 mol/dm^3
T_{nbp}	Normal boiling point temperature	225.06 K
ρ_{nbpv}	Vapor density at the normal boiling point	0.056 57 mol/dm^3
ρ_{nbpl}	Liquid density at the normal boiling point	12.611 mol/dm^3
T_0	Reference temperature for ideal gas properties	273.15 K
p_0	Reference pressure for ideal gas properties	0.001 MPa
h_0^0	Reference ideal gas enthalpy at T_0	41 266.39 J/mol
s_0^0	Reference ideal gas entropy at T_0 and p_0	236.1195 J/(mol·K)

1. Introduction

The development of equations of state for calculating the thermodynamic properties of fluids has progressed over the years from simple cubic and virial equations of state to Beattie–Bridgeman and Benedict–Webb–Rubin (BWR) equations, then to the modified BWR (mBWR) and to the fundamental equation of state explicit in the Helmholtz energy. Although the mBWR form can be converted to the Helmholtz energy form, the latter has advantages in terms of accuracy and simplicity. Most modern wide-range, high-accuracy equations of state for pure fluid properties are fundamental equations explicit in the Helmholtz energy as a function of density and temperature. All single-phase thermodynamic properties can be calculated as derivatives of the Helmholtz energy. The location of the saturation boundaries requires an iterative solution of the physical constraints on saturation (the so-called Maxwell criterion, i.e., equal pressures and Gibbs energies at constant temperature during phase changes). Thermodynamic consistency is maintained

by making saturation calculations using the equation of state (as opposed to using separate ancillary equations).

Recent equations of state show various degrees of accuracy, with the best approaching uncertainties of 0.01% in density over most of the accessible liquid and vapor states. Improvements have focused on increased accuracy, shorter equations, and improved representation of the critical region. However, in all these situations, equations are developed that exhibit behavior in the two phase region that is inconsistent with fluid behavior and that result in calculated values of pressure that are excessively high or low. Implicitly it has always been assumed that multiparameter equations of state are valid only outside their outermost spinodals. Comparisons of calculated values to data for single-phase state points and saturation conditions have been the traditional basis for establishing the accuracy of an equation of state. However, various mixture models use states in the two phase region of at least one of the pure fluid components in the calculation of the mixture properties. This need for more reliable calculated properties for inaccessible states inside the saturation boundaries prompted the development of a modified functional form for the equation of state explicit in Helmholtz energy. The new functional form developed in this work eliminates the oscillations with inappropriately high (both positive and negative) pressures in the two phase region calculated by other Helmholtz energy equations. The form is similar to that used in previous work, but includes modified terms that compensate for behavior attributable to the high numerical values of the exponents on the temperature terms in the equation at low temperatures. Details are given in Sec. 2.

The new functional form was applied to R-125 to incorporate new experimental measurements in the critical region (Perkins, 2002) and to take advantage of the wide coverage of published experimental data over the fluid surface. Refrigerant 125 (pentafluoroethane, HFC-125), and commercial blends containing R-125, are leading candidates for replacing the ozone-depleting hydrochlorofluorocarbon R-22 (chlorodifluoromethane, HCFC-22), the production of which will be phased out by the year 2020 under the terms of the Montreal Protocol. The thermodynamic properties of the refrigerant used as the working fluid significantly influence the energy efficiency and capacity of refrigeration systems, and accurate properties are essential in evaluating potential alternative refrigerants and in designing equipment.

In comparing the new functional form for R-125 with other equations, we have used the most accurate available equations of state for the comparisons. These equations are known for their ability to calculate accurate thermodynamic properties for single phase vapor and liquid states and saturation states. They form the base from which one can improve the next generation of equations of state, similar to work done by the research group at the Ruhr University in Bochum, Germany in improving the behavior of equations of state in the critical region of a pure fluid (Span and Wagner, 1996), which has inspired the work accomplished here. The physical characteristics (ideal behavior, extrapolation behavior, terms in the function form, etc.) of 34 equations of state for various fluids were compared with the characteristics of the new equation developed here for the refrigerant R-125. The fluids and the references to their respective equations of state are listed in Table 1, including the most recent equation for R-125 by Sunaga *et al.* (1998).

Although most pure compounds exist as an identifiable fluid only between its triple point temperature at the low extreme and by dissociation at the other extreme, every effort has been made to develop the functional form of the equation of state such that it allows the user to extrapolate to extreme limits of temperature, pressure, and density. At low temperatures, virial coefficients should approach negative infinity. At extremely high temperatures and densities, the equation should demonstrate proper fluid behavior, i.e., isotherms should not cross one another and pressures should not be negative. Although such limits exceed the boundaries of a normal fluid, there are applications where the boundaries may extend into such regions, and the equation of state should be capable of describing these situations. Calculated properties shown here at extreme conditions that are not defined by experiment are intended only for qualitative examination of the behavior of the equation of state, and exact accuracy estimates cannot be established in the absence of experimental data.

2. New Functional Form of the Equation of State

Modern equations of state are often formulated using the Helmholtz energy as the fundamental property with independent variables of density and temperature,

$$a(\rho,T)=a^0(\rho,T)+a^r(\rho,T), \tag{1}$$

where a is the Helmholtz energy, $a^0(\rho,T)$ is the ideal gas contribution to the Helmholtz energy, and $a^r(\rho,T)$ is the residual Helmholtz energy, which corresponds to the influence of intermolecular forces. Thermodynamic properties can be calculated as derivatives of the Helmholtz energy. For example, the pressure is

$$p=\rho^2\left(\frac{\partial a}{\partial \rho}\right)_T. \tag{2}$$

In practical applications, the functional form is explicit in the dimensionless Helmholtz energy, α, using independent variables of dimensionless density and temperature. The form of this equation is

$$\frac{a(\rho,T)}{RT}=\alpha(\delta,\tau)=\alpha^0(\delta,\tau)+\alpha^r(\delta,\tau), \tag{3}$$

where $\delta=\rho/\rho_c$ and $\tau=T_c/T$.

2.1. Properties of the Ideal Gas

The Helmholtz energy of the ideal gas is given by

$$a^0=h^0-RT-Ts^0. \tag{4}$$

The ideal gas enthalpy is given by

TABLE 1. Equations of state used for comparisons with the new functional form applied to R-125

Fluid	Reference	Equation type
Ammonia	Tillner-Roth *et al.* (1993)	Helmholtz
Argon	Tegeler *et al.* (1999)	Helmholtz[a]
Butane	Bücker and Wagner (2004)	Helmholtz[a]
Carbon Dioxide	Span and Wagner (1996)	Helmholtz[a]
Cyclohexane	Penoncello *et al.* (1995)	Helmholtz
Ethane	Bücker and Wagner (2004)	Helmholtz[a]
Ethylene	Smukala *et al.* (2000)	Helmholtz[a]
Fluorine	de Reuck (1990)	Helmholtz
Helium	McCarty and Arp (1990)	mBWR
Hydrogen	Younglove (1982)	mBWR
Isobutane	Bücker and Wagner (2004)	Helmholtz[a]
Methane	Setzmann and Wagner (1991)	Helmholtz[a]
Methanol	de Reuck and Craven (1993)	Helmholtz[b]
Neon	Katti *et al.* (1986)	Helmholtz
Nitrogen Trifluoride	Younglove (1982)	mBWR
Nitrogen	Span *et al.* (2000)	Helmholtz[a]
Oxygen	Schmidt and Wagner (1985)	Helmholtz
Propane	Miyamoto and Watanabe (2000)	Helmholtz
Propylene	Angus *et al.* (1980)	Helmholtz
R-11	Jacobsen *et al.* (1992)	Helmholtz
R-113	Marx *et al.* (1992)	Helmholtz
R-12	Marx *et al.* (1992)	Helmholtz
R-123	Younglove and McLinden (1994)	mBWR
R-124	de Vries *et al.* (1995)	Helmholtz
R-125	This Work	Helmholtz[a]
R-125	Sunaga *et al.* (1998)	Helmholtz
R-134a	Tillner-Roth and Baehr (1994)	Helmholtz
R-143a	Lemmon and Jacobsen (2000)	Helmholtz
R-152a	Outcalt and McLinden (1996)	mBWR
R-22	Kamei *et al.* (1995)	Helmholtz
R-23	Penoncello *et al.* (2003)	Helmholtz
R-32	Tillner-Roth and Yokozeki (1997)	Helmholtz
Sulfur Hexafluoride	de Reuck *et al.* (1991)	Helmholtz
Water	Wagner and Pruß (2002)	Helmholtz[a]
Air (as a pseudopure fluid)	Lemmon *et al.* (2000)	Helmholtz

[a]Contains additional terms for the critical region
[b]Contains additional terms to account for association in the vapor phase

$$h^0 = h_0^0 + \int_{T_0}^{T} c_p^0 \mathrm{d}T, \tag{5}$$

where c_p^0 is the ideal gas heat capacity. The ideal gas entropy is given by

$$s^0 = s_0^0 + \int_{T_0}^{T} \frac{c_p^0}{T}\mathrm{d}T - R\ln\left(\frac{\rho T}{\rho_0 T_0}\right), \tag{6}$$

where ρ_0 is the ideal gas density at T_0 and p_0 [$\rho_0 = p_0/(T_0 R)$], and T_0 and p_0 are arbitrary constants. Combining these equations results in the following equation for the Helmholtz energy of the ideal gas,

$$a^0 = h_0^0 + \int_{T_0}^{T} c_p^0 \mathrm{d}T - RT - T\left[s_0^0 + \int_{T_0}^{T} \frac{c_p^0}{T}\mathrm{d}T - R\ln\left(\frac{\rho T}{\rho_0 T_0}\right)\right]. \tag{7}$$

The ideal gas Helmholtz energy is given in a dimensionless form by

$$\alpha^0 = \frac{h_0^0 \tau}{RT_c} - \frac{s_0^0}{R} - 1 + \ln\frac{\delta\tau_0}{\delta_0\tau} - \frac{\tau}{R}\int_{\tau_0}^{\tau}\frac{c_p^0}{\tau^2}\mathrm{d}\tau + \frac{1}{R}\int_{\tau_0}^{\tau}\frac{c_p^0}{\tau}\mathrm{d}\tau, \tag{8}$$

where $\delta_0 = \rho_0/\rho_c$ and $\tau_0 = T_c/T_0$. The ideal gas Helmholtz energy is often reported in a simplified form for use in equations of state as

$$\alpha^0 = \ln\delta - \ln\tau + \sum a_k \tau^{i_k} + \sum a_k \ln[1 - \exp(-b_k\tau)]. \tag{9}$$

2.2. Properties of the Real Fluid

Unlike the ideal gas, the real fluid behavior is often described using empirical models that are only loosely supported by theoretical considerations. Although it is possible to extract values such as second and third virial coefficients from the fundamental equation, the terms in the equation are

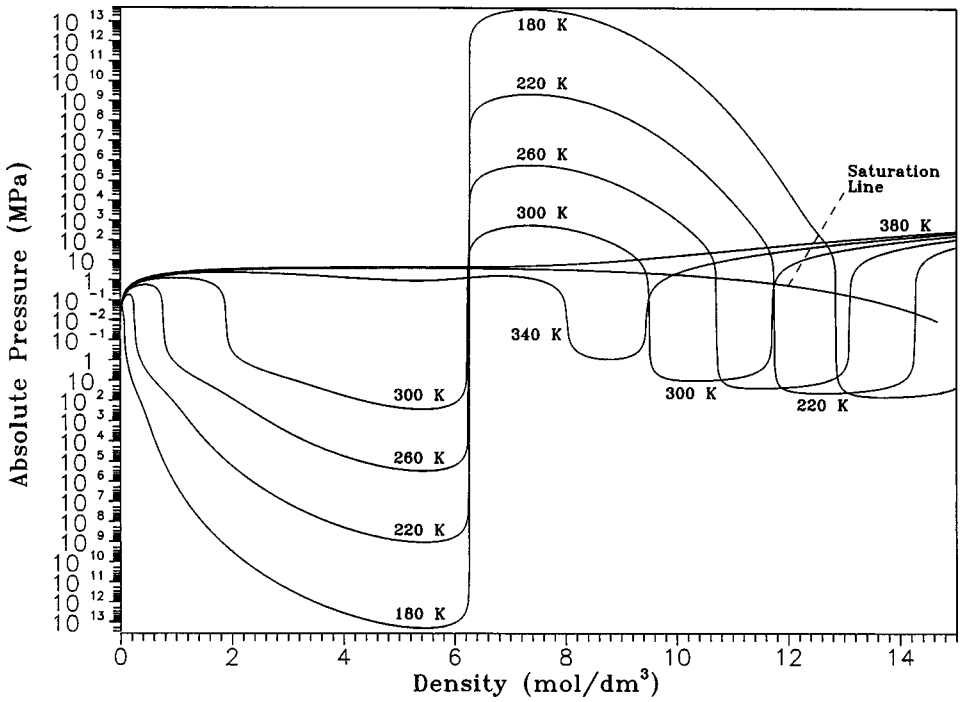

FIG. 1. Pressure–density diagram showing isotherms (from 180 to 400 K) in the two phase region for R-134a.

empirical, and any functional connection to theory is not entirely justified. The coefficients of the equation depend on the experimental data for the fitted fluid.

The common functional form for Helmholtz energy equations of state is

$$\alpha^r(\delta,\tau)=\sum N_k\delta^{d_k}\tau^{t_k}+\sum N_k\delta^{d_k}\tau^{t_k}\exp(-\delta^{l_k}), \tag{10}$$

where each summation typically contains 4–20 terms and where the index k points to each individual term. The new functional form developed in this work contains additional terms with exponentials of both density and temperature,

$$\alpha^r(\delta,\tau)=\sum N_k\delta^{d_k}\tau^{t_k}+\sum N_k\delta^{d_k}\tau^{t_k}\exp(-\delta^{l_k}) + \sum N_k\delta^{d_k}\tau^{t_k}\exp(-\delta^{l_k})\exp(-\tau^{m_k}). \tag{11}$$

Although the values of d_k, t_k, l_k, and m_k are arbitrary, t_k and m_k are generally expected to be greater than zero, and d_k and l_k are integers greater than zero. Functions for calculating pressures, energies, heat capacities, etc., as well as other derivative properties of the Helmholtz energy are given in Appendix A.

2.3. Implications of the New Terms in the Equation of State

Most multiparameter equations of state have shortcomings that affect the determination of phase boundaries or the calculation of metastable states within the two phase region. These can be traced to the use of the τ^t term in Eq. (10). As the temperature goes to zero, τ^t goes to infinity for values of $t>1$, causing the pressure to increase to infinity exponentially. The effect is more pronounced for higher values of t.

The primary use of these terms is for modeling the area around the critical region, where the properties change rapidly. Outside the critical region, the effect is damped out using the δ^d terms in the vapor and the $\exp(-\delta^l)$ terms in the liquid. Thus, at temperatures approaching the triple point temperature in the vapor phase, where the density is small, the higher the d in the δ^d part of each term, the smaller the range of influence of the exponential increase in temperature. Likewise, in the liquid at similar temperatures, a higher value of l damps out the effect of the τ^t part in the term. At densities near the critical density, $\delta^d\exp(-\delta^l)$ approaches a constant of around 0.4, and the shape of the τ^t contribution can greatly affect the critical region behavior of the model. Additional graphs and descriptions of these effects from different terms are given by Tillner-Roth (1998).

To demonstrate the behavior and magnitude of these terms at temperatures approaching the triple point, the path of a calculated isotherm at 180 K for R-134a is given in Fig. 1 and used here as a typical example. The equation of state for R-134a reaches its first maximum in pressure of 0.0406 MPa at the vapor spinodal of 0.0387 mol/dm^3. It then changes slope, reaching (at 5.44 mol/dm^3) a minimum pressure of -2.04×10^{13} MPa! It then quickly changes to positive values, reaching a maximum pressure of 4.21×10^{13} MPa at 7.38 mol/dm^3, and then drops down again, reaching another minimum pressure of -65.2 MPa at 13.7 mol/dm^3 at the liquid spinodal. Almost as soon as it becomes positive again, it

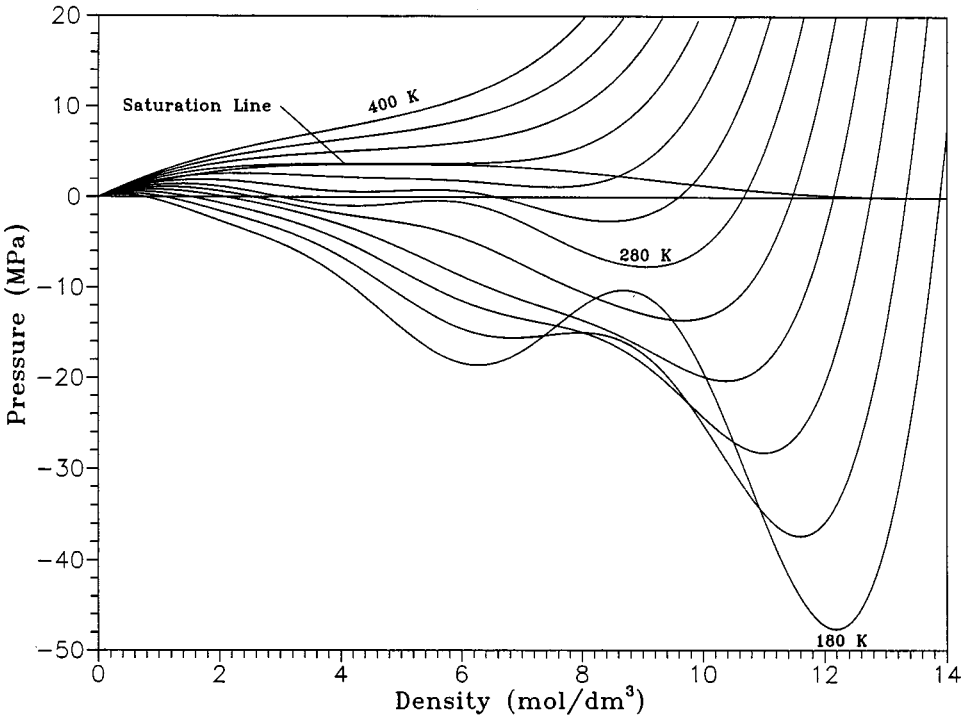

FIG. 2. Pressure–density diagram showing isotherms (from 180 to 400 K) in the two phase region for R-125.

reaches its vapor pressure of 0.00113 MPa at 15.33 mol/dm^3. The term in the R-134a equation responsible for these extreme values has a temperature exponent of $t=50$. Removing this term reduces the maximum pressure to 1.33×10^6 MPa. Although this behavior may seem absurd, it is typical of all multiparameter equations of state. The equation of state for water has a maximum pressure of 5.18×10^{20} MPa at 21.44 mol/dm^3 and 273.16 K. However, these maxima and minima in pressure are located well within the two phase region, and do not affect the accuracy of calculated properties in the single phase and along the saturation boundaries. They do, however, introduce multiple false roots—iteration routines that start with known values of temperature and pressure have the potential of finding the false roots, and the steep slopes can cause the routines to fail. There is also the possibility of adversely affecting mixture calculations that use metastable state information for the pure fluid constituents.

The introduction of the $\exp(-\tau^m)$ part of the equation of state damps out this effect as the temperature decreases. It allows the use of high values of the exponent t without large pressure fluctuations as described above. In the new equation for R-125 developed here, the highest value of t in the regular $\tau^t\delta^d\exp(-\delta^l)$ terms is 4.23. In the $\tau^t\delta^d\exp(-\delta^l)\times\exp(-\tau^m)$ terms, the highest value of t is 29. Since the new terms remove the large values resulting from the τ^{29} contributions at low temperatures, the maximum negative calculated pressure at 173 K is only -51.6 MPa at 12.39 mol/dm^3. In addition, this isotherm near the triple point temperature never crosses the zero pressure line except directly after passing through the vapor spinodal and right before passing through the saturated liquid state point. As shown in Fig. 2, it does exhibit incorrect changes in slope, but the oscillation never crosses the zero pressure line. This new form of the equation has eliminated the excessively large values of calculated pressure and the nearly infinite slopes of pressure with respect to density in the two phase region that are typical of other equations of state.

With the increased flexibility of the new terms comes the potential for degrading the behavior of the equation in the single-phase region. The heat capacities are especially sensitive to these new terms, and erroneous fluctuations can be created along the saturated liquid and vapor lines for values of these properties. In fitting equations, the correlator must take special care to examine the behavior of heat capacity and speed of sound to determine that the new terms have not adversely affected the equation. It is advisable to use as few of the new terms as possible, relying on the conventional terms with low values of t for fitting much of the thermodynamic surface in order to avoid inducing undesired characteristics in calculated values.

3. New Fitting Techniques in the Development of Equations of State

3.1. Fitting Procedures

The development of the equation of state is a process of correlating selected experimental data by least-squares fitting methods using a model that is generally empirical in nature, but is designed to exhibit proper limiting behavior in the ideal gas and low density regions and to extrapolate to tem-

peratures and pressures higher than those defined by experiment. In all cases, experimental data are considered paramount, and the proof of validity of any equation of state is evidenced by its ability to represent the thermodynamic properties of the fluid within the uncertainty of the experimental values. A secondary test of validity of an equation of state is its ability to extrapolate outside the range of experimental data. The selected data are usually a subset of the available database determined by the correlator to be representative of the most accurate values measured. The type of fitting procedure (e.g., nonlinear versus linear) determines how the experimental data will be used. In this work, a small subset of data was used in nonlinear fitting due to the extensive calculations required to develop the equation. The resulting equation was compared to all experimental data to verify that the data selection had been sufficient to allow an accurate representation of the available data.

One of the biggest advantages in nonlinear fitting is the ability to fit experimental data using nearly all the properties that were measured. For example, in linear fitting of the speed of sound, preliminary equations are required to transform measured values of pressure and temperature to the independent variables of density and temperature required by the equation of state. Additionally, the ratio c_p/c_v is required (also from a preliminary equation) to fit sound speed linearly. Nonlinear fitting can use pressure, temperature, and sound speed directly without any transformation of the input variables. Shock wave measurements of the Hugoniot curve are another prime example where nonlinear fitting can directly use pressure–density–enthalpy measurements without knowledge of the temperature for any given point. Another advantage in nonlinear fitting is the ability to use ''greater than'' or ''less than'' operators, such as in the calculation of two phase solutions (described below) or in controlling the extrapolation behavior of properties such as heat capacities or pressures at low or high temperatures. In linear fitting, only equalities can be used, thus curves are often extrapolated on paper by hand and ''data points'' are manually taken from the curves at various temperatures to give the fit the proper shape. With successive fitting, the curves are updated until the correlator is content with the final shape. In nonlinear fitting, curves can be controlled by ensuring that a calculated value along a constant property path is always greater (or less) than a previous value; thus magnitudes are not specified, only the shape. The nonlinear fitter then determines the best magnitude for the properties based on other information in a specific region.

Equations have been developed using linear regression techniques for several decades by fitting a comprehensive wide-range set of $p\rho T$ data, isochoric heat capacity data, linearized sound speed data (as a function of density and temperature), and second virial coefficients, as well as vapor pressures calculated from an ancillary equation. This process typically results in final equations with 25–40 terms. A cyclic process is sometimes used consisting of linear optimization, nonlinear fitting, and repeated linearization. Ideally this process is repeated until differences between the linear and nonlinear solutions are negligible. In certain cases, this convergence could not be reached—this led to the development of the ''quasi nonlinear'' optimization algorithm. However, since this algorithm still involves linear steps, it could not be used in combination with ''less than'' or ''greater than'' relations. Details about the linear regression algorithm can be found elsewhere (Wagner, 1974; Wagner and Pruß, 2002).

In the case of R-125, both methods were used to arrive at the final equation. Initial equations were developed using linear regression techniques. Once a good preliminary equation was obtained, nonlinear fitting techniques were used to shorten and improve upon it, fitting only a subset of the primary data used for linear fitting. The exponents for density and temperature, given in Eq. (11) as t_k, d_k, l_k, and m_k, were determined simultaneously with the coefficients of the equation. The nonlinear algorithm adjusted the parameters of the equation of state to reduce the overall sum of squares of the deviations of calculated properties from the input data, where the residual sum of squares was represented as

$$S=\sum W_\rho F_\rho^2+\sum W_p F_p^2+\sum W_{c_v} F_{c_v}^2+\ldots, \quad (12)$$

where W is the weight assigned to each data point and F is the function used to minimize the deviations. The equation of state was fitted to $p\rho T$ data using either deviations in pressure $F_p=(p_{\text{data}}-p_{\text{calc}})/p_{\text{data}}$ for vapor phase and critical region data, or as deviations in density, $F_\rho=(\rho_{\text{data}}-\rho_{\text{calc}})/\rho_{\text{data}}$, for liquid phase data. Since the calculation of density requires an iterative solution that extends calculation time during the fitting process, the nearly equivalent, noniterative form,

$$F_\rho=\frac{(p_{\text{data}}-p_{\text{calc}})}{\rho_{\text{data}}}\left(\frac{\partial\rho}{\partial p}\right)_T, \quad (13)$$

was used instead. Other experimental data were fitted in a like manner, e.g., $F_w=(w_{\text{data}}-w_{\text{calc}})/w_{\text{data}}$ for the speed of sound. The weight for each selected data point was individually adjusted according to type, region, and uncertainty. Typical values of W are 1 for $p\rho T$ and vapor pressure values, 0.05 for heat capacities, and 10–100 for vapor sound speeds. The values of the first and second derivatives of pressure with respect to density at the critical point were fitted so that the calculated values of these derivatives would be near zero at the selected critical point given in Eqs. (28)–(30).

To reduce the number of terms in the equation, terms were eliminated in successive fits by either deleting the term that contributed least to the overall sum of squares in the previous fit or by combining two terms that had similar values of the exponents (resulting in similar contributions to the equation of state). After a term was eliminated, the fit was repeated until the sum of squares for the resulting new equation was of the same order of magnitude as the previous equation. The final functional form for R-125 included 18 terms.

The exponents on density in the equation of state must be positive integers so that the derivatives of the Helmholtz

energy with respect to density have the correct theoretical expansion around the ideal gas limit. Since noninteger values for the density exponents resulted from the nonlinear fitting, a sequential process of rounding each density exponent to the nearest integer, followed by refitting the other parameters to minimize the overall sum of squares, was implemented until all the density exponents in the final form were integers. A similar process was used for the temperature exponents to reduce the number of significant figures to one or two past the decimal point.

In addition to reducing the number of individual terms in the equation compared to that produced by conventional linear least-squares methods, the extrapolation behavior of the shorter equations is generally more accurate, partially because there are fewer degrees of freedom in the final equation. In the longer equations, two or more correlated terms are often used to reproduce the accuracy of a single term in the nonlinear fit. The values of these correlated terms are often large in magnitude, and the behavior of the equation of state outside its range of validity, caused by incorporating such terms, is often unreasonable. Span and Wagner (1997) discuss the effects at high temperatures and pressures from intercorrelated terms.

3.2. Virial Coefficients

The Boyle temperature is the point at which the second virial coefficient, B, passes through zero. Below this point, B should be negative and constantly decreasing. Above the Boyle temperature, the second virial coefficient should increase to a maximum and then decrease to zero at very high temperatures. Calculated virial coefficients from most equations of state do not follow this behavior over all temperature ranges. Some oscillate around the zero line at temperatures below the fluid's triple point, and others increase monotonically at high temperatures, never reaching a maximum, and still others are negative at high temperatures. Of the 34 equations of state compared in this work (see Table 1), only the equations for ammonia, argon, butane, ethane, ethylene, isobutane, neon, nitrogen, propylene, R-23, and the equation for R-125 developed here conform to the proper behavior at both low and high temperatures. The oscillations at low temperatures are caused by the summation of several terms in the equation with high values of t and opposite signs on the coefficient. Several other equations (air, hydrogen, R-134a, and sulfur hexafluoride) have nearly correct shapes, except that B approaches a small positive constant value at high temperatures. At moderate temperatures below the triple point, where the second virial coefficients should decrease with decreasing temperature, the values of B calculated using some equations are positive and may oscillate about the zero line. Problems with the equation for oxygen extend above the triple point temperature.

The behavior of the third virial coefficient, C, should be similar to that of B, with C going to negative infinity at zero temperature, passing though zero at a moderate temperature, increasing to a maximum, and then approaching zero at extremely high temperatures. For the most part, those equations that behaved well for the second virial coefficient also behaved properly for the third. The equation for R-125 developed here conforms to appropriate behavior even at the very lowest temperatures. Additionally, the maximum in C occurred at a temperature near that of the critical point.

As an aid in visualization of the properties in the vapor phase and for limited use in low pressure applications, a truncated virial equation was developed for R-125 using the second and third virial coefficients,

$$Z = 1 + B\rho + C\rho^2 \tag{14}$$

or

$$\alpha^r = \rho_c B\,\delta + \rho_c^2 C\,\delta^2/2, \tag{15}$$

where B and C are

$$B = 1.4587\tau^{0.22} - 1.6522\tau^{0.42} - 0.075\,11\tau^4 \tag{16}$$

and

$$C = 0.029\,416\tau^3 - 0.004\,4202\tau^{10}. \tag{17}$$

A limited set of data in the vapor phase were used to fit the coefficients and exponents, and deviations of properties calculated using this equation are very similar to those from the full equation of state for R-125 (given later in this paper) for all temperatures and at densities less than 2 mol/dm^3. The shapes of B and C for the virial equation given here and for the full equation of state are shown in Figs. 3 and 4. For B, the shapes of the two equations deviate above the upper limit of the experimental data, but both still fulfill the general requirements outlined above. The differences in C for the two equations are more evident, although both meet the requirements specified earlier. Above 250 K, the values of C for both equations are less than 0.02 dm^6/mol^2, and the differences do not have a significant effect on calculated properties. Additional comparisons are made in the following section.

3.3. Vapor Phase Properties

One of the reasons for introducing the new terms was to eliminate undesirable effects of typical terms for states in the vapor phase. Examination of a graph of $(Z-1)/\rho$ versus density (such as that shown in Fig. 5) illustrates some of these problems. For such a graph, the y intercept values (values at zero density) are equivalent to the second virial coefficients. The slopes of the isotherms at zero density represent the third virial coefficients at that temperature. The fourth virial coefficients, D, are given by the curvatures of the isotherms. The curvature begins to play a role at densities that are about 20% of the critical density. At very low densities, ρ^3 in the virial expansion,

$$Z = 1 + B\rho + C\rho^2 + D\rho^3 + \ldots, \tag{18}$$

offsets the large numerical values of the fourth virial coefficient. However, with typical equations of state, the high powers of t in the temperature exponents lead to very large (positive or negative) values of D as the triple point is ap-

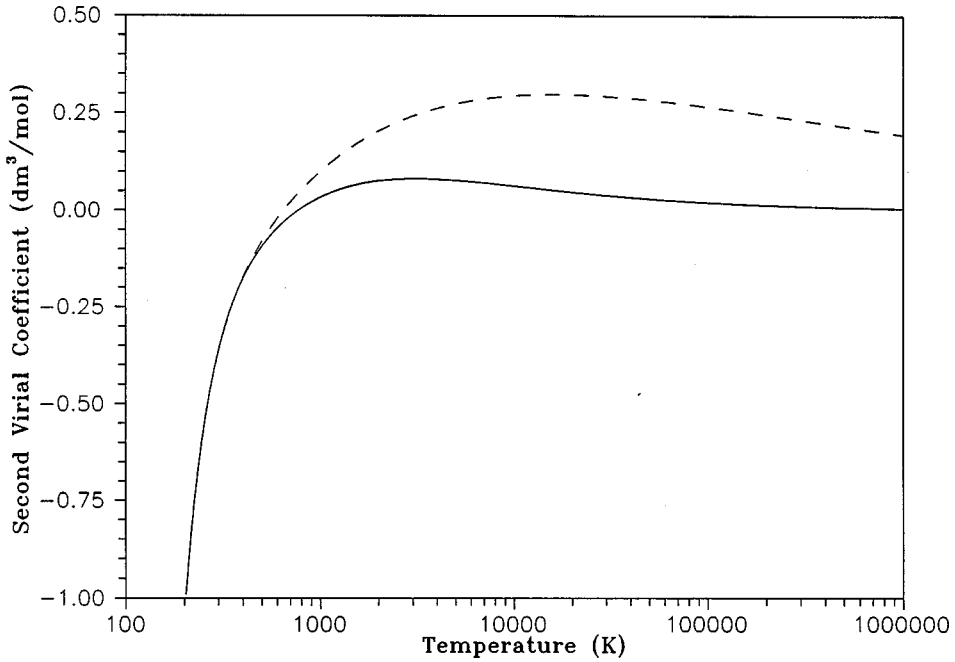

FIG. 3. Second virial coefficients from the virial equation (dashed line) and from the full equation of state (solid line).

proached, overwhelming the ability of ρ^3 to cancel the effect of the term from the virial expansion at low densities. This gives rise to curvature in the isotherms at very low densities at temperatures approaching the triple point. Figure 5 shows how this curvature affects the equation of Sunaga *et al.* (1998). The solid *lines* show the equation of state developed here. The long-dashed *curves* show the Sunaga equation. The short-dashed *lines* show the virial equation, Eq. (14). Figure 6 shows a plot of $(Z-1)/\rho$ over most of the surface of the R-125 equation of Sunaga *et al.* At low temperatures, the figure shows how the large oscillations in the equation result in the unwanted curvature of the isotherms at valid single-phase state points in the vapor phase. The same figure is shown in Fig. 7 for the equation of state for R-125 developed here, demonstrating the absence of the swings in the isotherms. There is some evidence of inappropriate maxima and

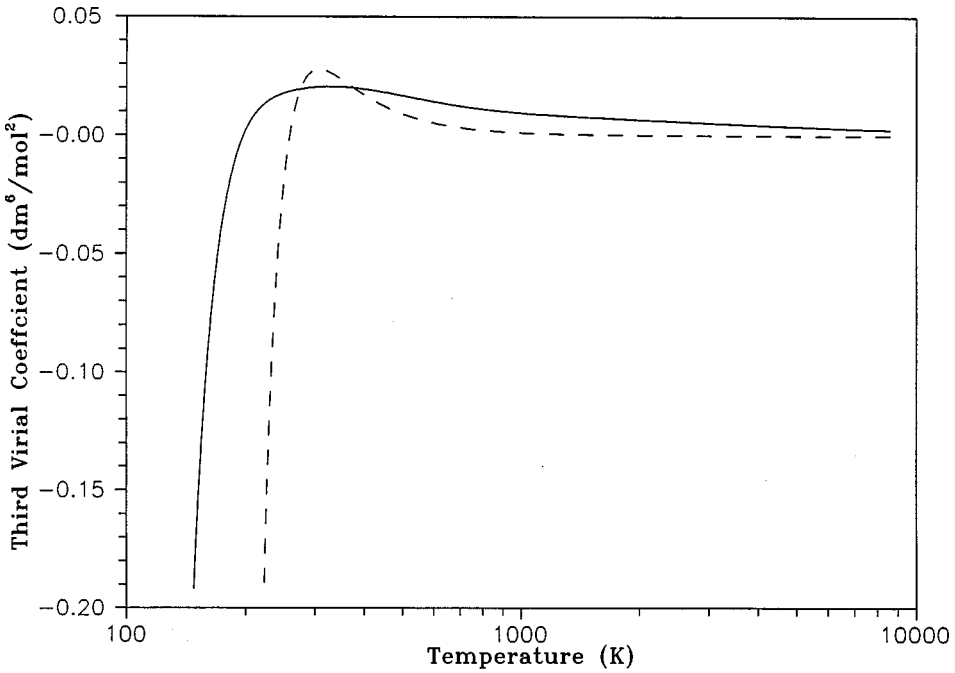

FIG. 4. Third virial coefficients from the virial equation (dashed line) and from the full equation of state (solid line).

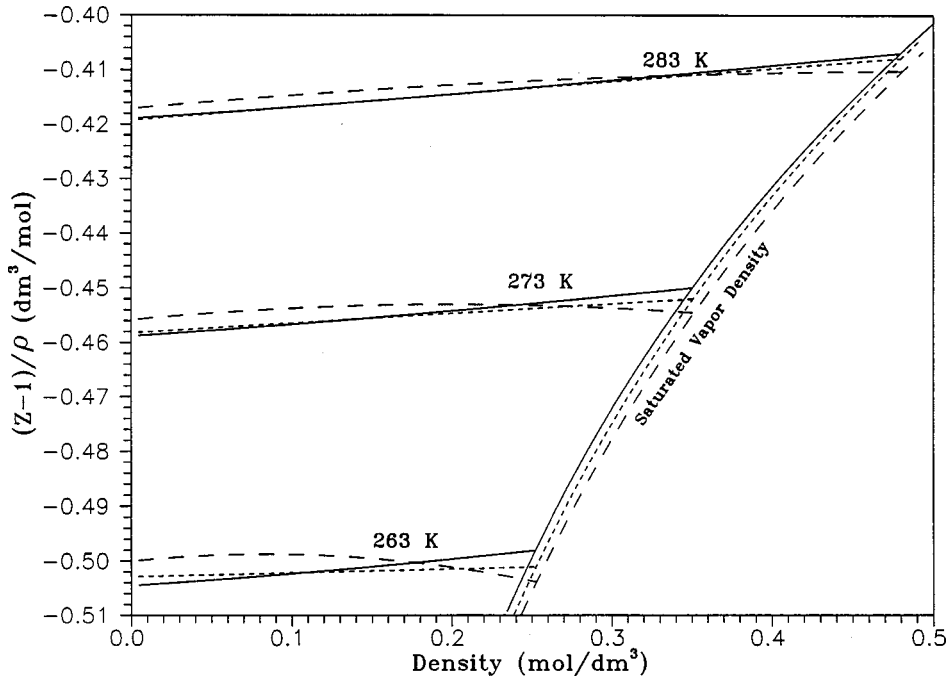

FIG. 5. Curvature of low temperature isotherms. Solid line—equation of state developed here; Short dashed line—Virial equation; Long dashed line—equation of Sunaga *et al.* (1998).

minima for this equation inside the two phase region, but the overall surface is much nearer the expected fluid behavior than that of other reference quality equations of state.

As the equation of state was developed, penalties were added to the objective function when a low temperature vapor isotherm began to show curvature. This was implemented by adding the square of the third derivative of the Helmholtz energy,

$$W\left(\frac{\partial^3 \alpha^r}{\partial \delta^3}\right)^2, \tag{19}$$

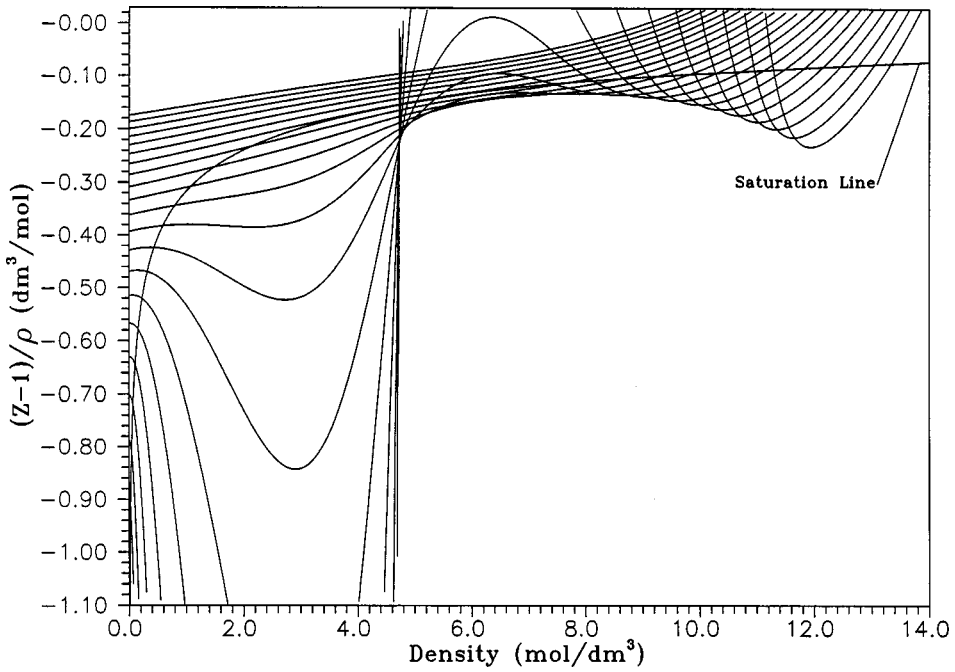

FIG. 6. $(Z-1)/\rho$ behavior in the two phase region of the Sunaga *et al.* equation of state for R-125. (Isotherms are drawn between 200 and 400 K in intervals of 10 K.)

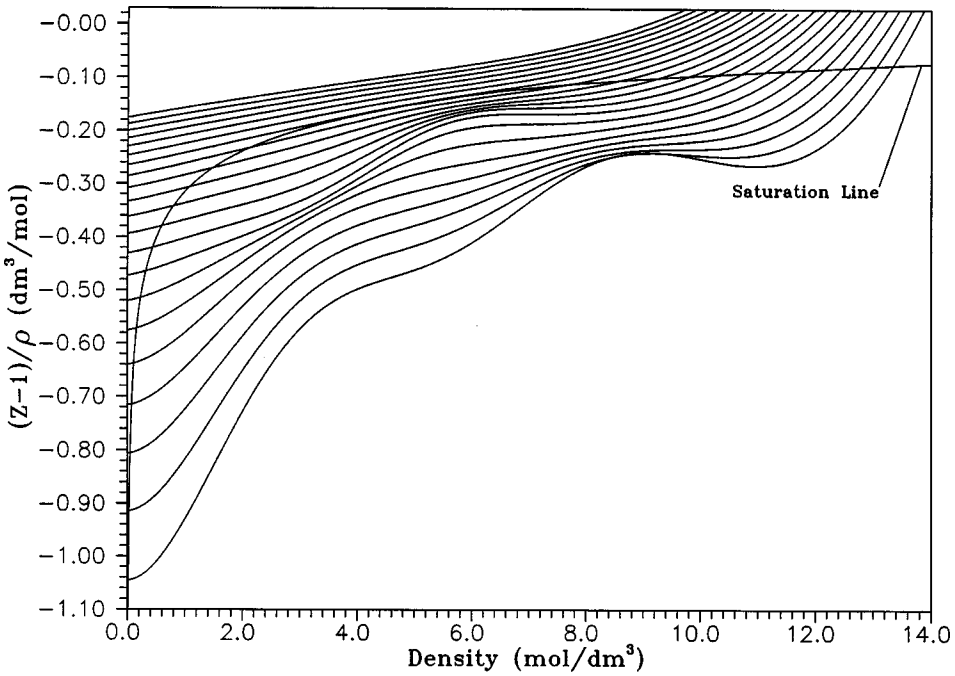

FIG. 7. $(Z-1)/\rho$ behavior in the two phase region of the equation of state for R-125 developed here. (Isotherms are drawn between 200 and 400 K in intervals of 10 K.)

to the sum of squares being minimized over a range of densities. The weight W was used to define how straight the isotherm should be, with a typical value of 100.

3.4. Two Phase Solutions

As equations of state become more complex to reach higher accuracies, the number of oscillations and their magnitudes generally increase within the two phase region. This can cause root solving routines to converge on the wrong root, resulting in erroneous answers. Certain techniques can be used in developing equations of state that ensure that additional erroneous roots do not occur along any particular isotherm. The work of Span (2000) highlighted the problems with limited accuracy in cubic equations and multiple loops in high accuracy equations of state.

Figure 8 shows a plot of the Helmholtz energy versus specific volume for R-143a calculated from the equation of state at 280 K. The oscillating curve shows the Helmholtz energy in either the single-phase or in the two phase region calculated directly from the equation as a function of temperature and density. The straight line connecting the saturation points is calculated using the quality, q,

$$a=(1-q)a_l+qa_v\,. \tag{20}$$

As described by Elhassan *et al.* (1997), saturation conditions can be calculated at the locations where a tangent line can be drawn connecting two points occurring along an isotherm. For R-143a, the plot shows that two solutions could be constructed, resulting in different calculated saturation pressures. (The saturation pressure is proportional to the slope of the tangent line.) Conversely, Fig. 9 for R-125 shows no indication of additional lines representing two phase states crossing the tangent line at saturation, i.e., only one line is simultaneously tangent to the curve at two points. The trends shown in this figure are evident in all isotherms down to the triple point temperature and beyond.

Elhassan *et al.* (1997) discussed these multiple maxima and minima and presented a fitting constraint that could be used only in nonlinear fitting:

$$a(v)-a_{\text{tang}}(v)\geqslant 0. \tag{21}$$

They applied this constraint to an equation for benzene, and had some success over a very limited range of temperatures, but were not able to apply the criterion over the full thermodynamic surface. The success of the new equation for R-125 in implementing Eq. (21) throughout the entire two phase region is based partly on the new functional form of the equation of state. In nonlinear fitting applications, this constraint can be implemented by requiring the first derivative of the Helmholtz energy with respect to density to decrease monotonically over a limited range of increasing vapor-like densities within the two phase region, effectively constraining the equation to have a single maximum in the region.

3.5. Near Critical Isochoric Heat Capacities

Although the new functional form introduced here has many advantages over other modern equations, it also has the potential to add unwanted bumps in the thermodynamic surface, especially for the isochoric and isobaric heat capacity. Figure 10 shows an example of a preliminary equation with a maximum in the liquid phase isochoric heat capacity along the 10 mol/dm^3 isochore. Other preliminary equations

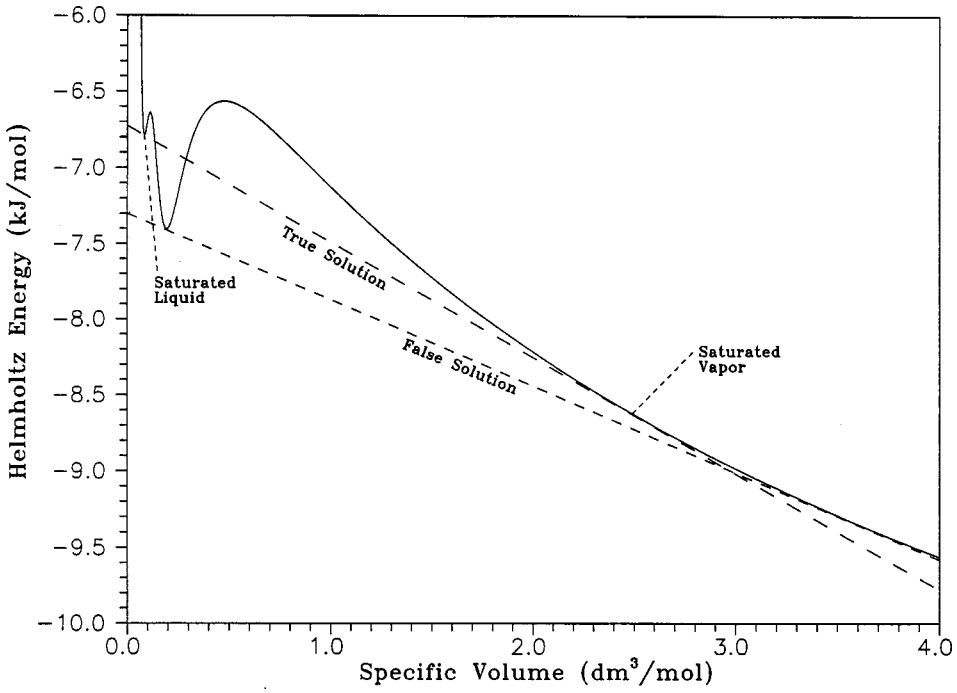

FIG. 8. Helmholtz energy-specific volume diagram of the 280 K isotherm in the single and two phase regions for R-143a.

showed inappropriate behavior, including bumps in different regions around the critical point. In order to eliminate the incorrect behavior, the value of the objective function was increased when the isochoric heat capacity decreased along an isochore (over a narrow range of temperatures where it should have increased), thereby removing any undesirable maximum in c_v in the final equation of state.

3.6. Pressure Limits at Extreme Conditions of Temperature and Density

The extrapolation behavior of a typical equation of state outside its physical bounds defined by experimental data can be problematic, with calculated pressures that are negative or that oscillate along an isotherm. Many equations have false

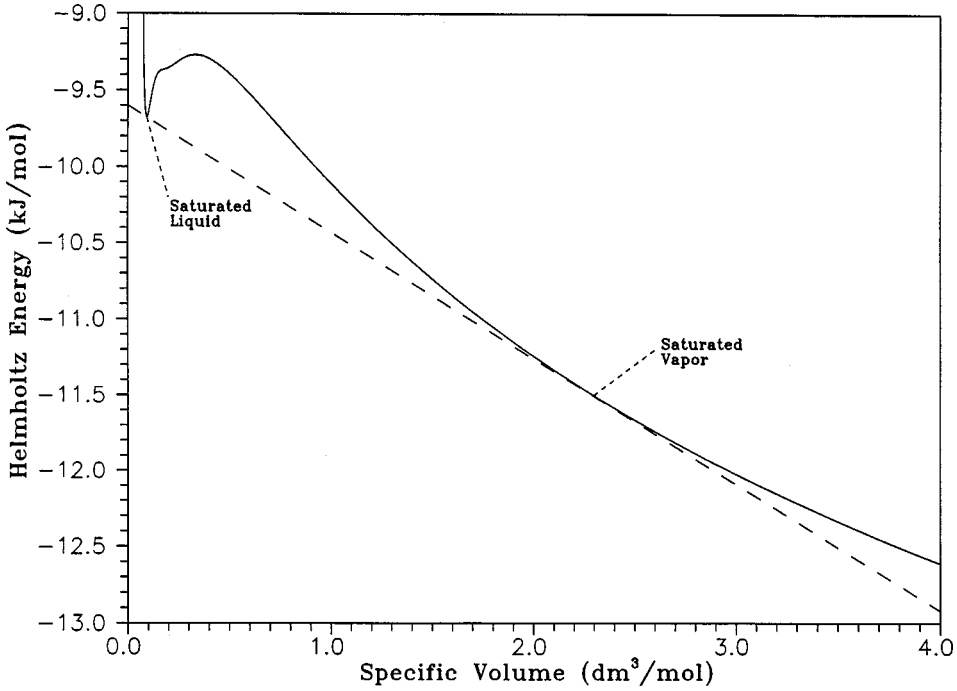

FIG. 9. Helmholtz energy-specific volume diagram of the 280 K isotherm in the single and two phase regions for R-125.

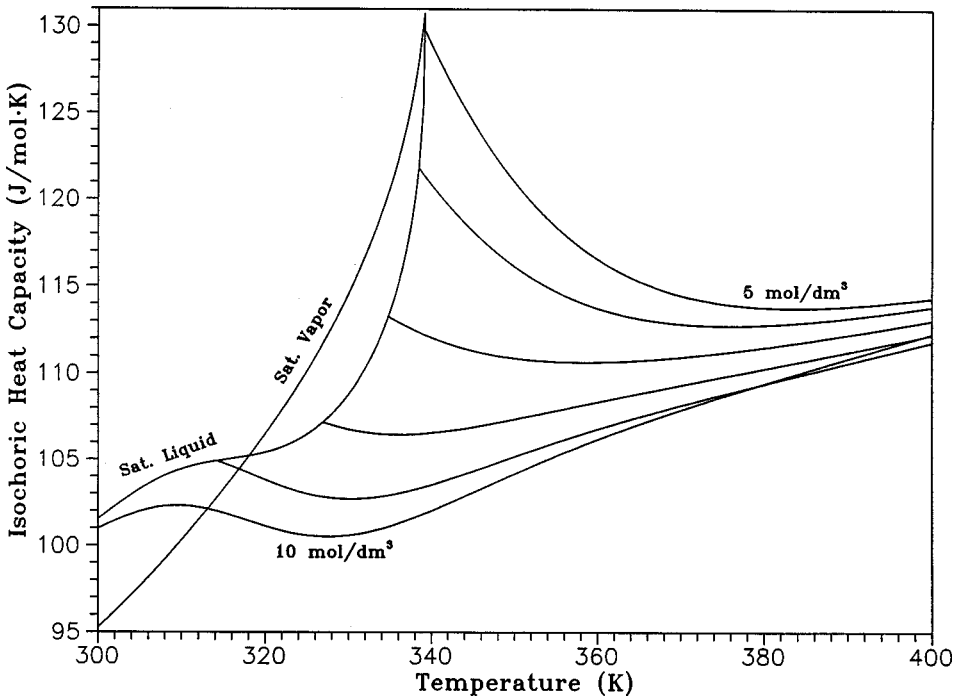

FIG. 10. Isochoric heat capacity diagram of a preliminary equation for R-125 showing incorrect behavior in the liquid phase. (Isochores are drawn at 5, 6, 7, 8, 9, and 10 mol/dm^3.)

roots outside their limits of validity that can trap root solving routines and return incorrect values. This is of even more concern when pure fluid equations are used in mixture models where extrapolation of the pure fluid equation is often a necessity. Other applications where inaccurate properties may cause problems include the calculation of shock tube properties and conditions where temperatures approach the dissociation limits of a compound. Several equations of state, such as those for nitrogen and carbon dioxide, were developed taking into account data to represent these shock tube conditions. In the case of metals, fluid conditions at extremely high values of temperature and pressure are of interest to some, and books can be found that describe such conditions, such as the SESAME databank of material properties (Holian, 1984). Conditions in the gas planets reach extreme values as well. Additional information about the extrapolation behavior of equations of state is given in Span and Wagner (1997).

The behavior of equations of state at extreme conditions varies incredibly; most have areas of negative pressures. Some, such as the equations for fluorine, hydrogen, oxygen, R-134a, and R-143a (see Table 1 for the list of citations to these equations of state) show behavior similar to that shown in Fig. 11 for ethylene. At high densities, the isotherms become parallel to one another. The equations for ammonia and R-11 show isotherms that cross. However, none of these equations exhibits the proper behavior. The SESAME databank shows examples of the proper shape of the isotherms at extreme conditions of pressure and density. In their plots, the isotherms all converge onto one line as the density increases. The point of convergence of an isotherm depends on its temperature, with higher temperatures converging onto the single line at higher densities. This can be seen in the case of the water equation of state if the term containing $t=0.375$ and $d=3$ is removed, as shown in Fig. 12. A similar plot for the equation for R-125 developed here is shown in Fig. 13.

The term responsible in the R-125 equation for the curves shown in Fig. 13 at high densities is $t=1$ and $d=4$ (the polynomial term with the highest value of d). Taking the partial derivative of the reduced Helmholtz energy for this term to solve for pressure,

$$p=\rho RT\left[1+\delta\frac{\partial\alpha^r}{\partial\delta}\right], \tag{22}$$

results in $4N_5\tau\delta^3$. Thus, at high densities and temperatures, the pressure converges to $p=N\delta^5$, where the constant N is $RdN_5T_c\rho_c$. The temperature dependence at extreme conditions is eliminated by the use of $t=1$ in this term. A value less than 1 causes the isotherms to become parallel, as seen with ethylene, fluorine, etc. A value greater than 1 causes the isotherms to cross, as is the case with ammonia and R-11. The value of the coefficient of this term should always be positive. For $d=3$ (and $t=1$), the increase in pressure would be less (by a factor of δ), than that shown in Fig. 13.

Some of the bumps that appear in various equations come from the excess use of the polynomial terms—those without the exponential parts. A minimum number of these terms should be used; in the equation for R-125, only five are used: three to represent the second virial coefficients ($d=1$), one for the third virial coefficient ($d=2$), and the term for the

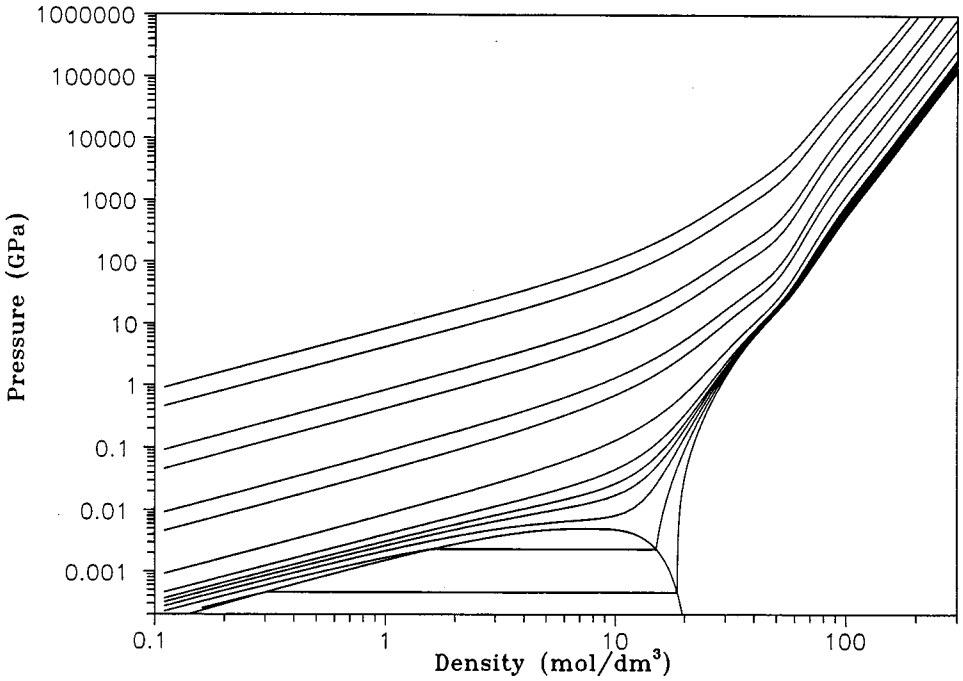

FIG. 11. Isothermal behavior of the ethylene equation of state at extreme conditions of temperature and pressure. (Isotherms are shown at 200, 250, 300, 350, 400, 500, 1000, 5000, 10 000,..., 1 000 000 K.)

extreme conditions ($d=4$). Constraints on the number of terms were first introduced during the development of the equation of state for carbon dioxide (Span and Wagner, 1996) and were explained in more detail by Span and Wagner (1997). During the development of the water equation of state (Wagner and Pruß, 2002), the maximum number of polynomial terms allowed in any particular fit was limited to 12 (with the final fit containing only seven polynomial terms). Values calculated with the $N\delta^d\tau^t\exp(-\delta^l)$ terms diminish at state points away from the critical density. These terms are more suitable for equation of state modeling. Figure 13 shows the behavior of the new equation and the absence of any inappropriate trends at extreme conditions of pressure, density, and temperature.

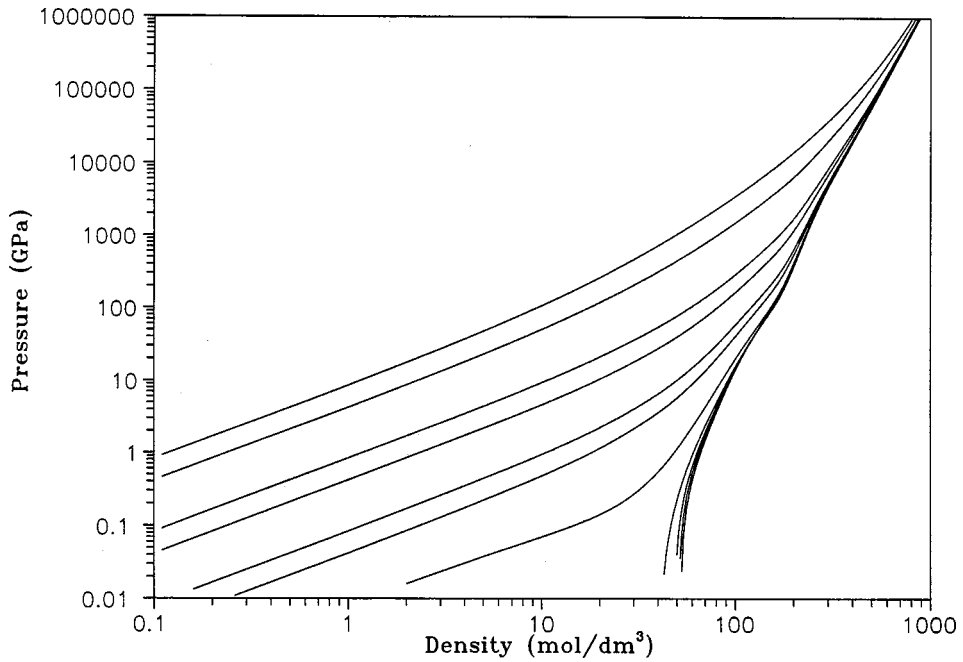

FIG. 12. Isothermal behavior of a modified water equation of state at extreme conditions of temperature and pressure. (Isotherms are shown at 200, 250, 300, 350, 400, 500, 1000, 5000, 10 000,..., 1 000 000 K.)

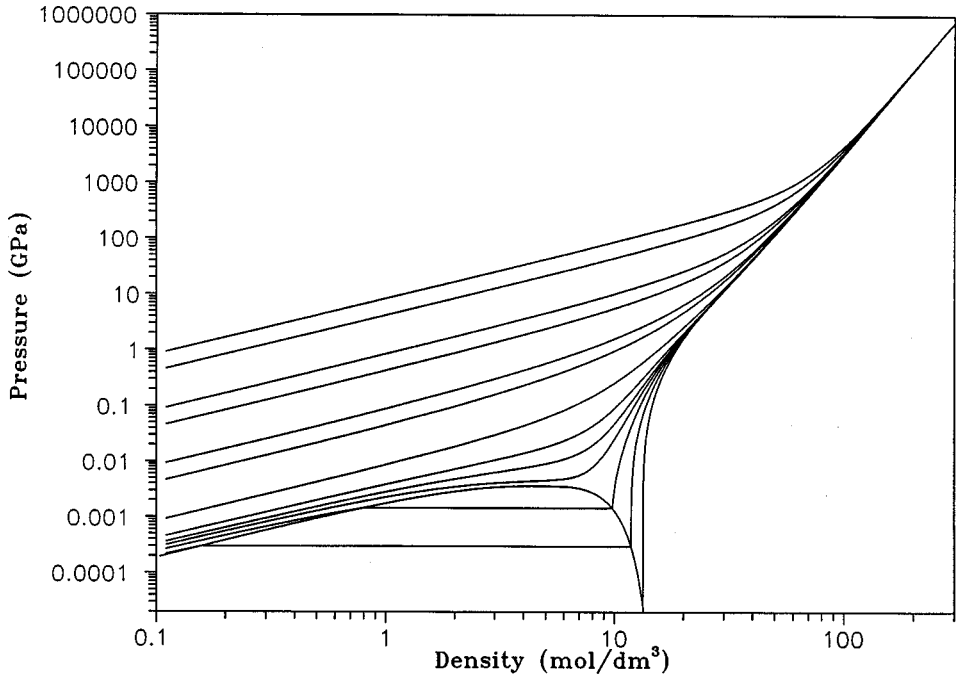

FIG. 13. Isothermal behavior of the R-125 equation of state developed in this work at extreme conditions of temperature and pressure. (Isotherms are shown at 200, 250, 300, 350, 400, 500, 1000, 5000, 10 000,..., 1 000 000 K.)

3.7. Ideal Curves

Plots of certain characteristic curves are useful in assessing the behavior of an equation of state in regions away from the available data (Deiters and de Reuck, 1997, Span and Wagner, 1997, Span, 2000). The characteristic curves are the Boyle curve, given by the equation

$$\left(\frac{\partial Z}{\partial v}\right)_T = 0, \tag{23}$$

the Joule–Thomson inversion curve,

$$\left(\frac{\partial Z}{\partial T}\right)_p = 0, \tag{24}$$

the Joule inversion curve,

$$\left(\frac{\partial Z}{\partial T}\right)_v = 0, \tag{25}$$

and the ideal curve,

$$\frac{p}{\rho RT} = 1. \tag{26}$$

The temperature at which the Boyle and ideal curves begin (at zero pressure) is also known as the Boyle temperature, or the temperature at which the second virial coefficient is zero. The point at zero pressure along the Joule inversion curve corresponds to the temperature at which the second virial coefficient is at a maximum. (Thus, in order for the Joule inversion curve to extend to zero pressure, the second virial coefficient must pass through a maximum value, a criterion which is not followed by all equations of state.) Although the curves do not provide numerical information, reasonable shapes of the curves, as shown for R-125 in Fig. 14, indicate qualitatively correct extrapolation behavior of the equation of state extending to high pressures and temperatures far in excess of the likely thermal stability of the fluid. Of all the equations studied in this work (see Table 1), only the equations of argon, butane, carbon dioxide, ethane, ethylene, isobutane, neon, nitrogen, R-143a, R-23, water, and air showed qualitatively correct behavior for the ideal curves. Most of these were fitted using either shock tube data or empirical criteria to correct the behavior of the equation. The equation for R-124, shown in Fig. 15, demonstrates undesirable shapes of the ideal curves. The behavior of properties on the ideal curves should be analyzed during the development of the equation. Additional figures showing the ideal curves for argon, nitrogen, methane, ethane, oxygen, carbon dioxide, water, and helium are given in Span and Wagner (1997).

Equation of state terms with values of $t<0$ have a negative effect on the shapes of the ideal curves. The effects of all terms should be damped at high temperatures, but with $t<0$, the contribution to the equation increases as the temperatures rises. Negative temperature exponents should never be allowed in an equation of state of the form presented in this work. Unfortunately, around half of the equations available to the authors used at least one negative temperature exponent.

4. Application to Pentafluoroethane (R-125)

Several equations of state for R-125 have been previously developed by various researchers worldwide. The equation

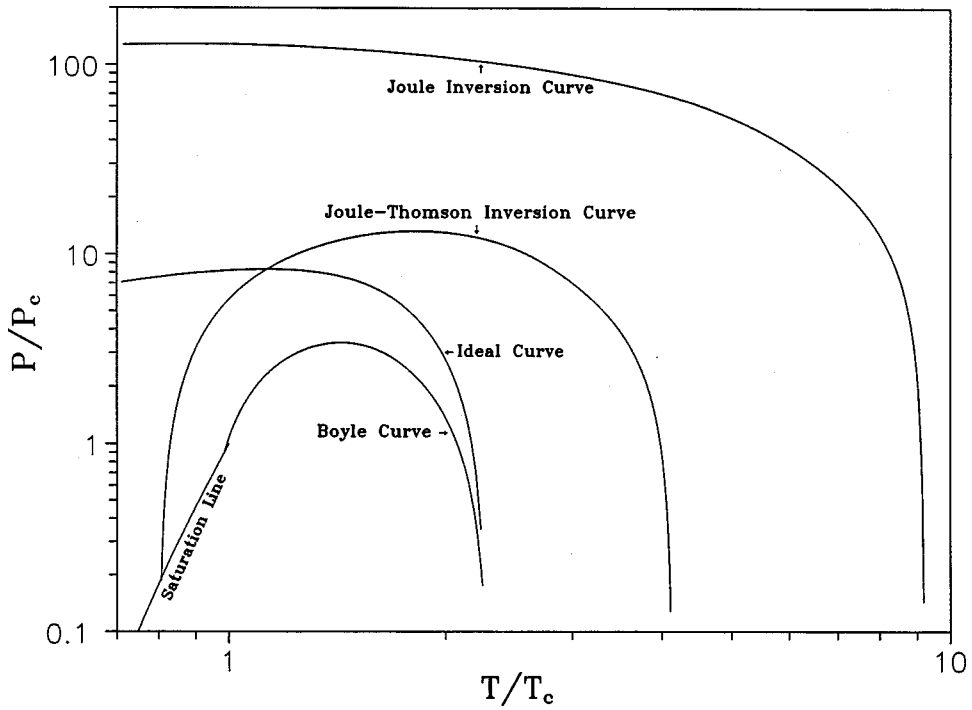

FIG. 14. Characteristic (ideal) curves of the equation of state for R-125.

of Sunaga *et al.* (1998) is an 18-term equation explicit in Helmholtz energy, the equation of Piao and Noguchi (1998) is a 20-term modified Benedict–Webb–Rubin equation, the equation of Outcalt and McLinden (1995) is a 32-term modified Benedict–Webb–Rubin equation, and the equation of Ely (1995) is a 27-term equation explicit in Helmholtz energy. The equation of Piao and Noguchi (1998) was selected by Annex 18 of the Heat Pump Program of the International Energy Agency (IEA) in 1996 as an international standard formulation for use by the refrigeration industry. The equa-

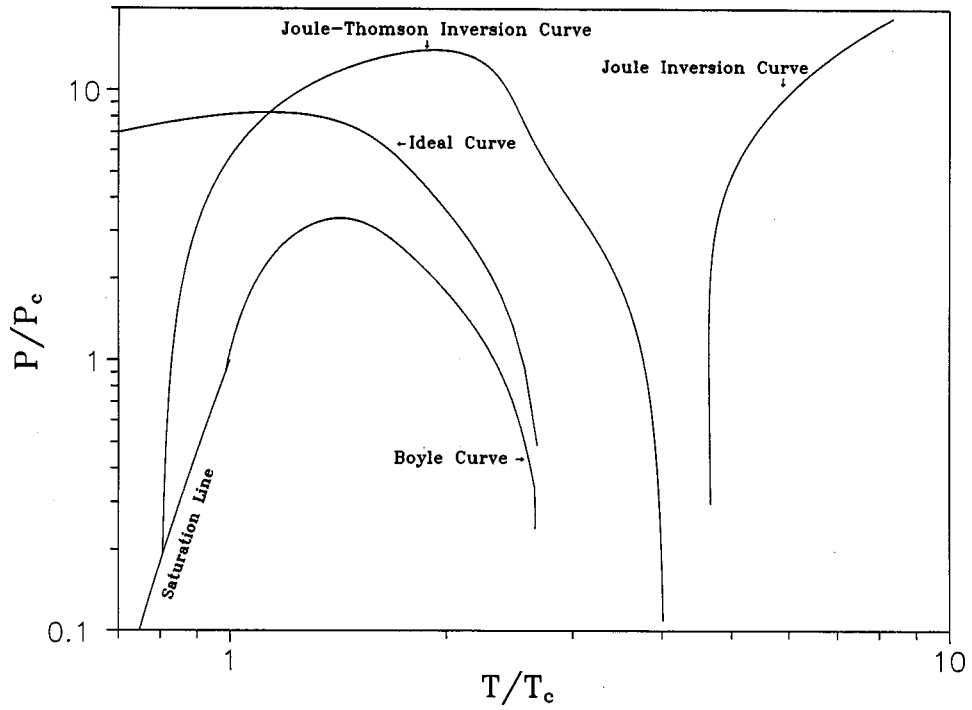

FIG. 15. Characteristic (ideal) curves of the equation of state for R-124.

TABLE 2. Summary of critical point parameters

Author	Critical temp. (K)	Critical pressure (MPa)	Critical density (kg/m^3)	Critical density (mol/dm^3)
Duarte-Garza *et al.* (1997)	339.41	3.6391	572.26	4.768
Fukushima and Ohotoshi (1992)	339.18	3.621	562.	4.6825
Higashi (1994)	339.17	3.62	572.	4.7658
Kuwabara *et al.* (1995)	339.165		568.	4.7325
Nagel and Bier (1993)	339.43	3.635	568.	4.7325
Schmidt and Moldover (1994)	339.33		565.	4.7075
Singh *et al.* (1991)	339.45	3.6428	570.98	4.7573
Wilson *et al.* (1992)	339.1725	3.595	571.3	4.7600
Values Adopted in this Work	**339.173**	**3.6177**		**4.779**

tion of Sunaga *et al.* (1998) became available shortly thereafter, and has been used as the primary equation for R-125 since that time.

The new equation presented here is an 18-term fundamental equation explicit in the reduced Helmholtz energy. The range of validity of the equation of state for R-125 is from the triple point temperature (172.52 K) to 500 K at pressures to 60 MPa. In addition to the equation of state, ancillary functions were developed for the vapor pressure and for the densities of the saturated liquid and saturated vapor. These ancillary equations can be used as initial estimates in computer programs for defining the saturation boundaries, but are not required to calculate properties from the equation of state.

The units adopted for this work were Kelvins (ITS-90) for temperature, megapascals for pressure, and moles per cubic decimeter for density. Units of the experimental data were converted as necessary from those of the original publications to these units. Where necessary, temperatures reported on IPTS-68 were converted to the International Temperature Scale of 1990 (ITS-90) (Preston-Thomas, 1990). The $p\rho T$ and other data selected for the determination of the coefficients of the equation of state are described later along with comparisons of calculated properties to experimental values to verify the accuracy of the model developed in this research. Data used in fitting the equation of state for R-125 were selected to avoid redundancy in various regions of the surface.

4.1. Critical and Triple Points

Critical parameters for R-125 have been reported by various authors and are listed in Table 2. The difficulties in the experimental determination of the critical parameters are the probable cause of considerable differences among the results obtained by the various investigators. The critical density is difficult to determine accurately by experiment because of the infinite compressibility at the critical point and the associated difficulty of reaching thermodynamic equilibrium. Therefore, reported values for the critical density are often calculated by power-law equations, by extrapolation of rectilinear diameters using measured saturation densities, or by correlating single-phase data close to the critical point. The critical temperature used in this work was obtained by fitting the data of Kuwabara *et al.* (1995) and Higashi (1994) at temperatures above 324 K to the equation

$$\frac{\rho_\sigma}{\rho_c} - 1 = N_1\left(1 - \frac{T_\sigma}{T_c}\right) \pm N_2\left(1 - \frac{T_\sigma}{T_c}\right)^\beta, \qquad (27)$$

where $T_c = 339.173$ K, $\rho_c = 4.779$ mol/dm^3, $N_1 = 0.981\,36$, $N_2 = 1.9125$, $\beta = 0.334\,14$, T_σ is the saturation temperature, and ρ_σ is the saturation density for the liquid or the vapor. The critical density and critical temperature were fitted simultaneously with the coefficients of the equation. Equation (27) is valid only in the critical region at temperatures above 330 K. Calculated values from this equation are shown in Fig. 16 along with experimental data along the saturation lines, with the lower plot showing a smaller region close to the critical point.

The critical pressure was determined from the equation of state at the critical temperature and density. The resulting values of the critical properties are

$$T_c = 339.173 \text{ K}, \qquad (28)$$

$$\rho_c = 4.779 \text{ mol/dm}^3, \qquad (29)$$

and

$$p_c = 3.6177 \text{ MPa}. \qquad (30)$$

These values should be used for all property calculations with the equation of state. The selected critical temperature agrees well with the values reported by both Kuwabara *et al.* (339.165 K) and Higashi (339.17 K).

The triple point temperature of R-125 was measured by Lüddecke and Magee (1996) by slowly applying a constant heat source to a frozen sample contained within the cell of an adiabatic calorimeter and noting the sharp break in the temperature rise, resulting in

$$T_{tp} = 172.52 \text{ K}, \qquad (31)$$

measured on the ITS-90 temperature scale. The value of the triple point pressure calculated from the equation of state is $p_{tp} = 2.914$ kPa.

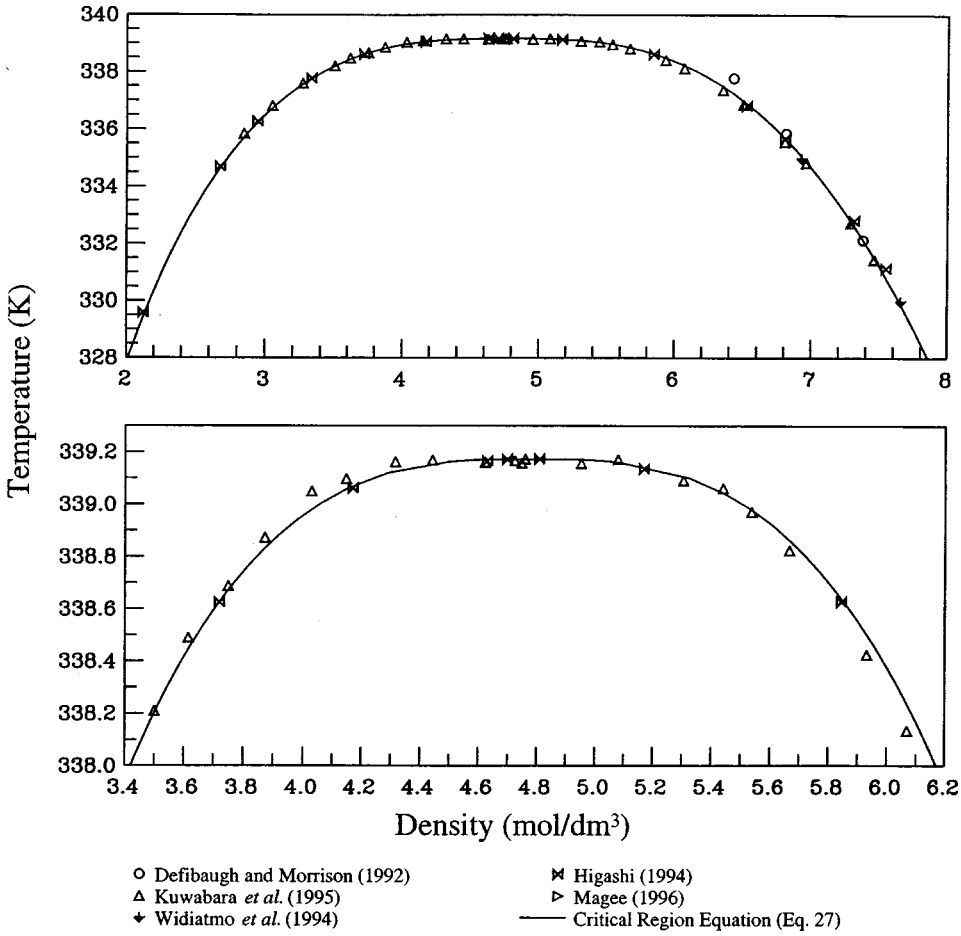

FIG. 16. Critical region saturation data.

4.2. Vapor Pressures

Table 3 summarizes the available vapor pressure data for R-125. The vapor pressure can be represented with the ancillary equation

$$\ln\left(\frac{p_\sigma}{p_c}\right)=\frac{T_c}{T}[N_1\theta+N_2\theta^{1.5}+N_3\theta^{2.3}+N_4\theta^{4.6}], \quad (32)$$

where $N_1=-7.5295$, $N_2=1.9026$, $N_3=-2.2966$, $N_4=-3.4480$, $\theta=(1-T/T_c)$, and p_σ is the vapor pressure. The values of the coefficients and exponents were determined using nonlinear least squares fitting techniques. The values of the critical parameters are given above in Eqs. (28)–(30).

4.3. Saturated Densities

Table 4 summarizes the saturated liquid and vapor density data for R-125. The saturated liquid density is represented by the ancillary equation

$$\frac{\rho'}{\rho_c}=1+N_1\theta^{1/3}+N_2\theta^{0.6}+N_3\theta^{2.9}, \quad (33)$$

where $N_1=1.6684$, $N_2=0.884\,15$, $N_3=0.443\,83$, $\theta=(1-T/T_c)$, and ρ' is the saturated liquid density. The saturated vapor density is represented by the equation

$$\ln\left(\frac{\rho''}{\rho_c}\right)=N_1\theta^{0.38}+N_2\theta^{1.22}+N_3\theta^{3.3}+N_4\theta^{6.9}, \quad (34)$$

where $N_1=-2.8403$, $N_2=-7.2738$, $N_3=-21.890$, $N_4=-58.825$, and ρ'' is the saturated vapor density. Values calculated from the equation of state using the Maxwell criteria were used in developing Eq. (34), and deviations between the equation of state and the ancillary equation are generally less than 0.03% below 337.5 K and less than 0.3% at higher temperatures. The values of the coefficients and exponents for Eqs. (33) and (34) were also determined using nonlinear least squares fitting techniques.

4.4. Equation of State

The critical temperature and density required in the reducing parameters for the equation of state given in Eq. (3) are 339.173 K and 4.779 mol/dm^3. The ideal gas reference state points are $T_0=273.15$ K, $p_0=0.001$ MPa, $h_0^0=41\,266.39$ J/mol, and $s_0^0=236.1195$ J/(mol·K). The values for h_0^0 and s_0^0 were chosen so that the enthalpy and entropy of

TABLE 3. Summary of vapor pressure data

Author	No. of points	Temp. range (K)	AAD (%)
Baroncini *et al.* (1993)	58	235–333	0.062
Boyes and Weber (1995)	29	273–335	0.019
de Vries (1997)	98	222–339	0.030
Duarte-Garza *et al.* (1997)	15	220–337	0.204
Duarte-Garza and Magee (1997)	12	172–225	0.038
Gorenflo *et al.* (1996)	25	233–337	0.061
Lee *et al.* (2000)	3	293–313	0.167
Lüddecke and Magee (1996)	8	180–250	0.285
Magee (1996)	34	180–335	0.209
Monluc *et al.* (1991)	23	303–339	0.056
Nagel and Bier (1993)	18	205–339	0.521
Oguchi *et al.* (1996)	61	223–338	0.081
Sagawa (1994)	23	313–339	0.080
Sagawa *et al.* (1994)	26	308–339	0.042
Tsvetkov *et al.* (1995)	34	263–338	0.055
Weber and Silva (1994)	114	175–284	0.027
Widiatmo *et al.* (1994)	20	219–334	0.324
Wilson *et al.* (1992)	39	195–339	0.451
Ye *et al.* (1995)	12	290–339	0.070

TABLE 4. Summary of saturated liquid and vapor density data

Author	No. of points	Temp. range (K)	AAD (%)
Saturated Liquid Density Data			
Defibaugh and Morrison (1992)	9	275–337	0.376
Higashi (1994)	9	324–339	0.830
Kuwabara *et al.* (1995)	16	331–339	1.313
Magee (1996)	7	173–308	0.102
Widiatmo *et al.* (1994)	25	219–334	0.076
Saturated Vapor Density Data			
Higashi (1994)	8	326–339	0.752
Kuwabara *et al.* (1995)	13	335–339	1.748

the saturated liquid state at 0 °C are 200 kJ/kg and 1 kJ/(kg·K), respectively, corresponding to the common convention in the refrigeration industry.

In the calculation of the thermodynamic properties of R-125 using an equation of state explicit in the Helmholtz energy, an equation for the ideal gas heat capacity, c_p^0, is needed to calculate the Helmholtz energy for the ideal gas, α^0. Values of the ideal gas heat capacity derived from low pressure experimental heat capacity or speed of sound data are given in Table 5 along with theoretical values from statistical methods using fundamental frequencies. Differences between the different sets of theoretical values arise from the use of different fundamental frequencies and from the models used to calculate the various couplings between the vibrational modes of the molecule. The equation for the ideal gas heat capacity for R-125, used throughout the remainder of this work, was developed by fitting values reported by Yokozeki *et al.* (1998), and is given by

$$\frac{c_p^0}{R} = 3.063T^{0.1} + 2.303\frac{u_1^2 \exp(u_1)}{[\exp(u_1)-1]^2} + 5.086\frac{u_2^2 \exp(u_2)}{[\exp(u_2)-1]^2} + 7.300\frac{u_3^2 \exp(u_3)}{[\exp(u_3)-1]^2}, \tag{35}$$

where u_1 is 314 K/T, u_2 is 756 K/T, u_3 is 1707 K/T, and the ideal gas constant, R, is 8.314 472 J/(mol·K) (Mohr and Taylor, 1999). The Einstein functions containing the terms u_1, u_2, and u_3 were used so that the shape of a plot of the ideal gas heat capacity versus temperature would be similar to that derived from statistical methods. However, these are empirical coefficients and should not be confused with the fundamental frequencies. Comparisons of values calculated using Eq. (35) to the ideal gas heat capacity data are given in Fig. 17. The ideal gas Helmholtz energy equation, derived from Eqs. (8) and (35), is

$$\alpha^0 = \ln\delta - \ln\tau + a_1 + a_2\tau + a_3\tau^{-0.1} + a_4\ln[1-\exp(-b_4\tau)] + a_5\ln[1-\exp(-b_5\tau)] + a_6\ln[1-\exp(-b_6\tau)], \tag{36}$$

where $a_1 = 37.2674$, $a_2 = 8.884\,04$, $a_3 = -49.8651$, $a_4 = 2.303$, $b_4 = 0.925\,78$, $a_5 = 5.086$, $b_5 = 2.228\,95$, $a_6 = 7.3$, and $b_6 = 5.032\,83$.

The coefficients N_k of the residual part of the equation of state [given in Eq. (11) and repeated below] are given in Table 6.

$$\alpha^r(\delta,\tau) = \sum_{k=1}^{5} N_k\delta^{d_k}\tau^{t_k} + \sum_{k=6}^{15} N_k\delta^{d_k}\tau^{t_k}\exp(-\delta^{l_k}) + \sum_{k=16}^{18} N_k\delta^{d_k}\tau^{t_k}\exp(-\delta^{l_k})\exp(-\tau^{m_k}) \tag{37}$$

5. Experimental Data and Comparisons to the Equation of State

During the last several years, many experimental studies of the thermodynamic properties of R-125 have been reported, e.g., $p\rho T$ properties, saturation properties, critical parameters, heat capacities, speeds of sound, second virial co-

TABLE 5. Summary of ideal gas heat capacity data

Author	No. of points	Temp. range (K)	AAD (%)
Experimental Data			
Gillis (1997)	8	240–380	0.067
Grigiante *et al.* (2000)	7	260–360	0.153
Hozumi *et al.* (1996)	6	273–343	0.799
Theoretical Values			
Chen *et al.* (1975)	18	100–1500	0.860
Yokozeki *et al.* (1998)	45	120–1000	0.014

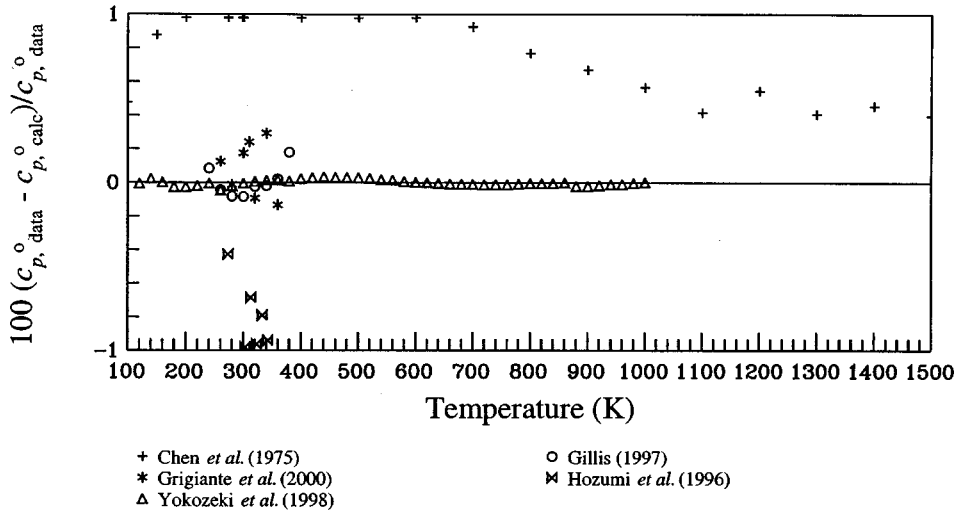

FIG. 17. Comparisons of ideal gas heat capacities calculated with the ancillary equation to experimental and theoretical data.

efficients, and ideal gas heat capacities. Selected data were used for the development of the new thermodynamic property formulation reported here. Comparisons were made to all available experimental data, including those not used in the development of the equation of state.

The accuracy of the equation of state was determined by statistical comparisons of calculated property values to experimental data. These statistics are based on the percent deviation in any property, X, defined as

$$\%\Delta X = 100\left(\frac{X_{\text{data}} - X_{\text{calc}}}{X_{\text{data}}}\right). \tag{38}$$

Using this definition, the average absolute deviation (AAD) is defined as

$$\text{AAD} = \frac{1}{n}\sum_{i=1}^{n} |\%\Delta X_i|, \tag{39}$$

TABLE 6. Parameters and coefficients of the equation of state

k	N_k	d_k	t_k	l_k	m_k
1	5.280 760	1	0.669		
2	−8.676 580	1	1.05		
3	0.750 1127	1	2.75		
4	0.759 0023	2	0.956		
5	0.014 518 99	4	1.00		
6	4.777 189	1	2.00	1	
7	−3.330 988	1	2.75	1	
8	3.775 673	2	2.38	1	
9	−2.290 919	2	3.37	1	
10	0.888 8268	3	3.47	1	
11	−0.623 4864	4	2.63	1	
12	−0.041 272 63	5	3.45	1	
13	−0.084 553 89	1	0.72	2	
14	−0.130 8752	5	4.23	2	
15	0.008 344 962	1	0.20	3	
16	−1.532 005	2	4.5	2	1.7
17	−0.058 836 49	3	29.0	3	7.0
18	0.022 966 58	5	24.0	3	6.0

where n is the number of data points. The average absolute deviations between experimental data and calculated values from the equation of state are given in the tables summarizing the data. In Tables 3 and 4 for saturation values, measured properties are compared with the equation of state, not with the ancillary equations. The comparisons given in the sections below for the various datasets compare values calculated from the equation of state to the experimental data using the average absolute deviations given by Eq. (39). Discussions of maximum errors or of systematic offsets use the absolute values of the deviations.

5.1. Comparisons with Saturation Data

Figure 18 shows comparisons of vapor pressures calculated from the equation of state with experimental data. The dashed lines in these figures represent the ancillary equation, Eq. (32). The maximum deviation between the vapor pressure ancillary equation and the equation of state is 0.03%. When calculating vapor pressures from the equation of state (not from the ancillary equations), the average deviations are less than 0.1% for the datasets of Baroncini *et al.* (1993), Boyes and Weber (1995), de Vries (1997), Duarte-Garza and Magee (1997), Gorenflo *et al.* (1996), Monluc *et al.* (1991), Oguchi *et al.* (1996), Sagawa *et al.* (1994), Weber and Silva (1994), and Ye *et al.* (1995). Comparisons with the equation of Sunaga *et al.* (1998) are also shown in Fig. 18. Their equation is very similar to that presented here at temperatures above 250 K, but tends to follow the data of de Vries (1997) at lower temperatures. The data of de Vries show trends at low temperatures different from those of Duarte-Garza and Magee and of Weber and Silva. The Duarte-Garza and Magee values were derived from caloric information in the two phase region; they agree well with the data of Weber and Silva measured with ebulliometer techniques (with a small offset of 0.05%). Consistent with a decision made by the IEA-Annex 18 for R-143a (see Lemmon and Jacobsen,

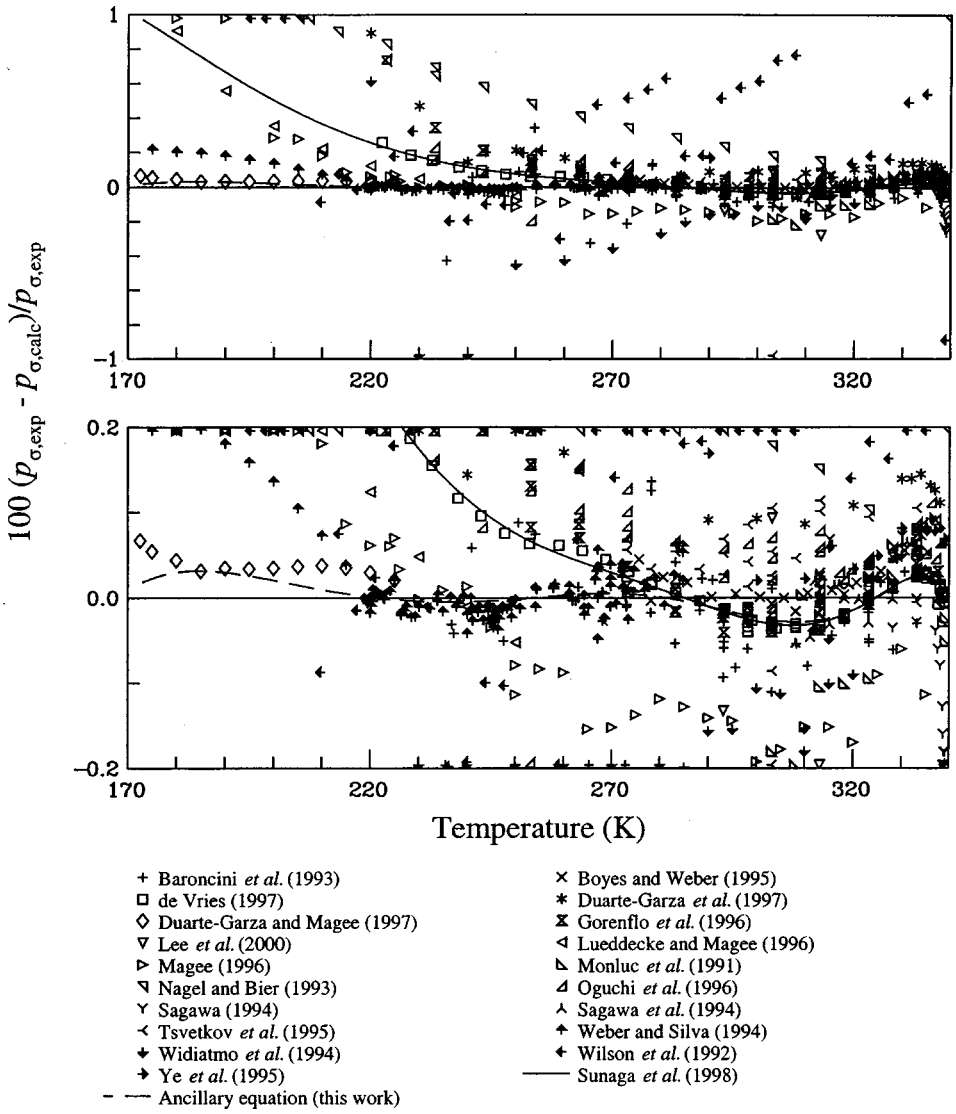

FIG. 18. Comparisons of vapor pressures calculated with the equation of state to experimental data.

2000), the vapor pressure values of Duarte-Garza and Magee (1997) were believed to be the most reliable values available at low temperatures.

Figure 19 shows comparisons of saturated liquid densities calculated from the equation of state with experimental data. Deviations of calculated values from data increase as the critical region is approached. This region is shown in detail in Fig. 20, which displays both saturated liquid and saturated vapor densities in the critical region. There are no saturated vapor density data outside the critical region. The dashed lines in these figures represent the ancillary equations reported in Eqs. (33) and (34). In the critical region, the equation of state agrees well with the data of Kuwabara *et al.* (1995) and Higashi (1994), with increasing deviations as the critical point is approached (between 4 and 5 mol/dm^3). Near a density of 6 mol/dm^3, the equation shows an offset of about 1% with the data of Kuwabara *et al.* However, the power law equation used to represent these and other critical region data showed the same tendency as the equation of state, even though fitted with completely different parameters and input data. Although not entirely conclusive, this behavior supports the decision made by the authors in representing the saturation properties for R-125. The model favors the data of Higashi (1994) but the uncertainty of calculated values includes the values of Kuwabara *et al.* (1995).

5.2. $p\rho T$ Data and Virial Coefficients

The experimental $p\rho T$ data for R-125 are summarized in Table 7 and shown graphically in Fig. 21. For clarity, data in the critical region are shown in Fig. 22. Figure 23 compares densities calculated from the equation of state with experimental data, and Fig. 24 compares pressures calculated from the equation of state with the experimental data in the extended critical region of R-125. In these figures, data of a given type are separated into temperature increments of 10 K outside the critical region; the temperatures listed at the top of each small plot are the lower bounds of the data in the

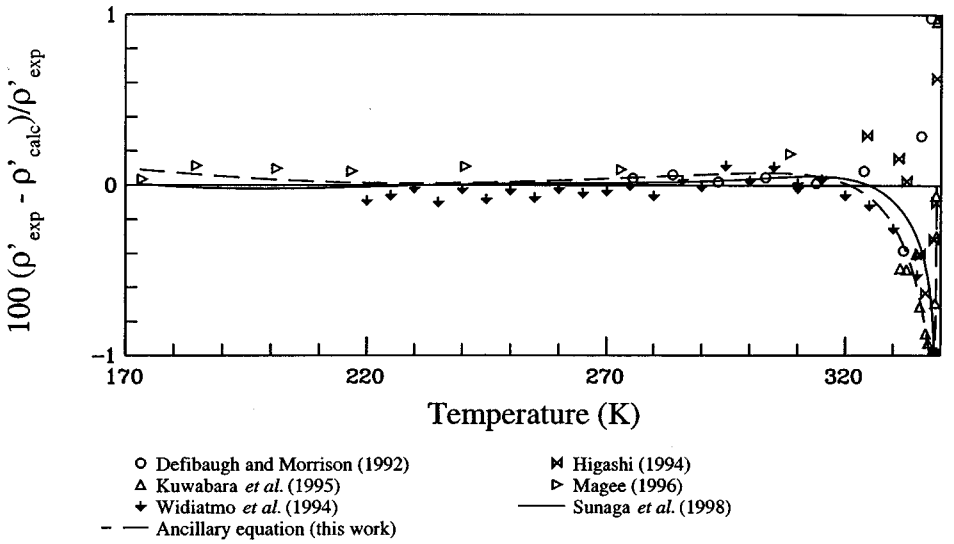

FIG. 19. Comparisons of saturated liquid densities calculated with the equation of state to experimental data.

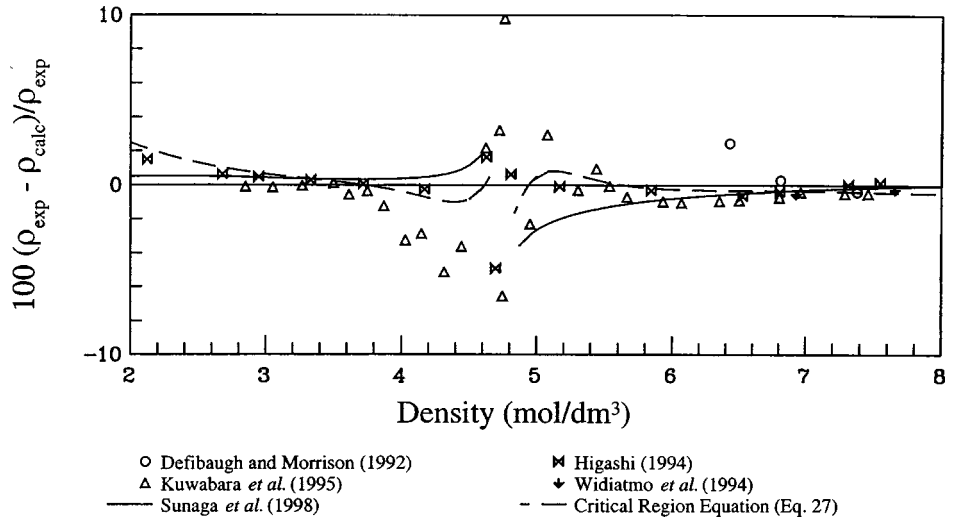

FIG. 20. Comparisons of saturated liquid and vapor densities in the critical region calculated with the equation of state to experimental data.

TABLE 7. Summary of $p\rho T$ data

Source	No. of points	Temp. range (K)	Pressure range (MPa)	Density range (mol/dm^3)	AAD (%)
Baroncini *et al.* (1993)	58	293–338	0.99–2.52	0.50–1.29	0.389
Boyes and Weber (1995)	92	273–363	0.33–4.56	0.12–2.83	0.056
de Vries (1997)	962	243–413	0.02–19.8	0.01–12.6	0.072
Defibaugh and Morrison (1992)	162	275–369	1.59–6.33	2.15–11.2	0.697
Duarte-Garza *et al.* (1997)	148	180–350	1.24–67.9	7.62–14.2	0.089
Magee (1996)	77	178–398	3.58–35.4	9.29–14.0	0.034
Monluc *et al.* (1991)	50	310–423	1.57–11.1	0.81–7.83	0.700
Oguchi *et al.* (1996)	167	280–473	0.81–17.0	0.42–9.54	0.956
Perkins (2002)	1483	301–428	2.88–19.7	3.13–9.96	0.105
Sagawa *et al.* (1994)	211	308–423	0.69–11.8	0.30–8.87	0.977
Takahashi *et al.* (1999)	131	298–423	0.10–8.40	0.03–4.77	0.513
Tsvetkov *et al.* (1995)	44	273–443	0.60–6.09	0.30–4.31	0.799
Wilson *et al.* (1992)	84	198–448	1.73–10.4	0.89–13.6	1.382
Ye *et al.* (1995)	93	290–390	0.12–3.55	0.04–1.91	0.115
Zhang *et al.* (1996)	93	290–390	0.12–3.55	0.04–1.91	0.075

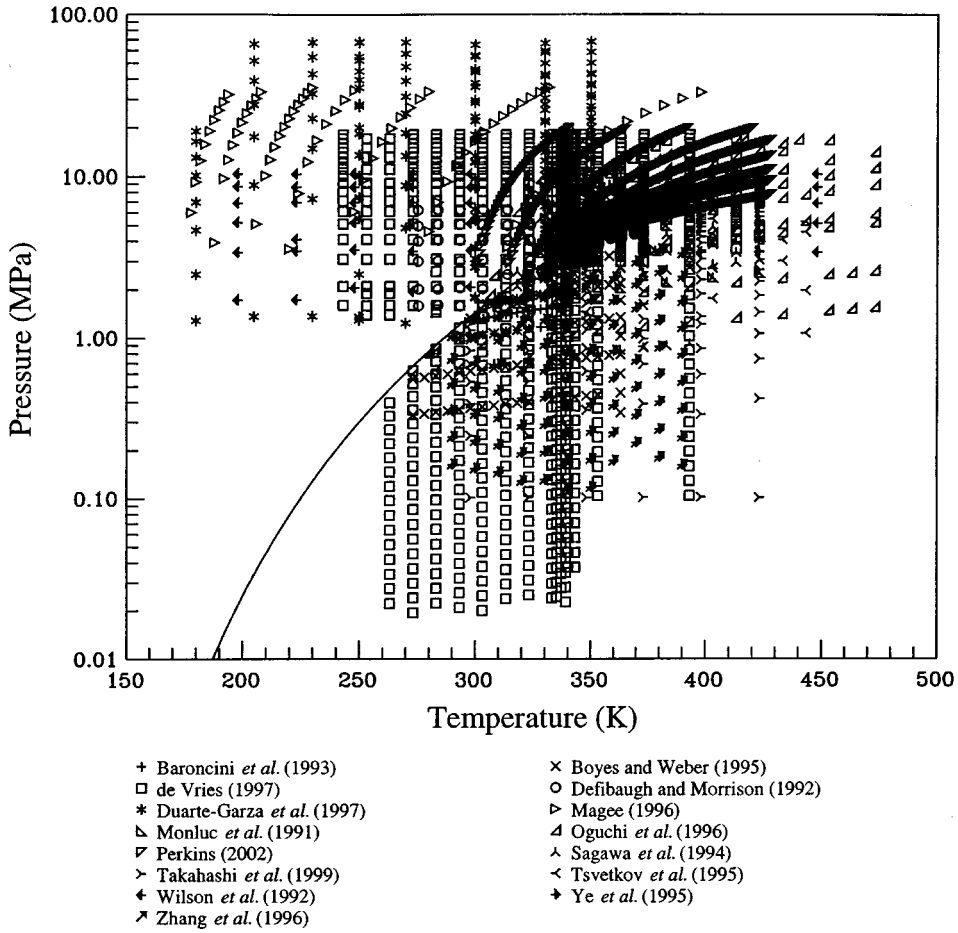

FIG. 21. Experimental $p\rho T$ data.

plots, and the comparisons to the equation of state of Sunaga *et al.* (solid lines in the plots) are given at this temperature.

Below 270 K, the equation of state represents the data of Magee (1996), Duarte-Garza *et al.* (1997), and de Vries (1997) with deviations in density generally less than 0.05%. Between 270 and 330 K in the liquid, density deviations are slightly higher for the data of Duarte-Garza *et al.* and Perkins (2002), and somewhat lower (0.02%) for the data of de Vries and for Defibaugh and Morrison (1992). In the vapor phase up to 330 K, the datasets are not as consistent as are those in the liquid, and density deviations tend to be higher, except for the data of de Vries, which is represented by an AAD of 0.018%. Deviations for other datasets in this region are 0.12% for Zhang *et al.* (1996), 0.08% for Boyes and Weber (1995), and 0.17% for Ye *et al.* (1995). Omitting the data in the region between 3 and 7 mol/dm^3 and at temperatures up to 360 K (i.e., the critical region), the spread in the data at higher temperatures continues to increase, and the deviations remain under 0.1% for only the datasets of de Vries, Zhang *et al.*, Ye *et al.*, Boyes and Weber, Magee, and Perkins. Of particular interest in this region are the data of Perkins, with more than 1200 data points spanning pressures up to 20 MPa and temperatures up to 429 K. Deviations of density values calculated using the equation of state from these data are within about 0.04% in this region.

In the critical region omitted above, from 3 to 7 mol/dm^3 with temperatures to 360 K, deviations in density are no longer a useful comparison since the uncertainty in the dependent variable pressure (and to a certain degree temperature) becomes the dominant contribution to the total uncertainty in density. Comparisons of calculated values with even the most accurate data show average deviations of 0.4% (de Vries) and 0.85% (Perkins) with maximum errors exceeding 5% in density. In order to compare the equation of state with experimental data in this region, deviations in pressure are more meaningful, and the following discussion uses such deviations as a basis for the discussion of the accuracy of the representation of experimental values by the equation of state where the slopes of the isotherms on $p-\rho$ coordinates are essentially flat. Figure 24 compares values from the equation to data in a limited region around the critical point. Most of the data in this region are represented with average deviations of 0.1%. The scatter in the data is similar for most of the datasets with deviations of calculated values from the data of de Vries of about 0.06%. Average deviations for comparisons with other datasets are 0.19% for Perkins, 0.27% for Sagawa *et al.* (1994), and 0.31% for Defibaugh and Morri-

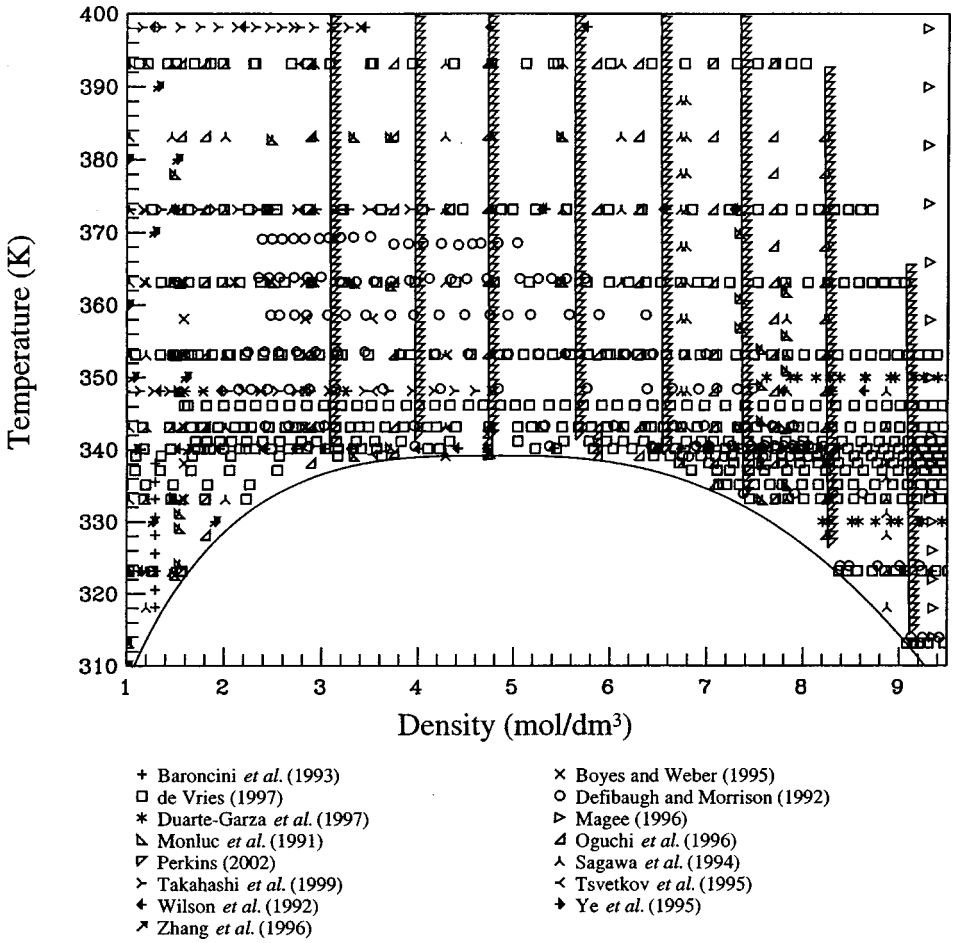

FIG. 22. Experimental $p\rho T$ data in the critical region.

son. The maximum deviation from the data of de Vries is 0.22%.

Table 8 summarizes the sources for the second virial coefficients of R-125. Additional values for the second virial coefficient were numerically determined by fitting $(Z-1)/\rho$ as a function of density using the data of de Vries (1997). The additional data (values at zero density) are shown in Fig. 25 as circles. These values are given in Table 9. Data below 0.1 mol/dm^3 were not used because such low density data may be subject to larger errors due to local adsorption onto the walls of the apparatus or to higher uncertainties in the measurement of extremely low pressures. Additional information about the high uncertainties in the second virial coefficients at low temperatures was reported by Wagner and Pruß (2002). The solid lines show isotherms calculated from the equation of state presented here and the solid curve represents the saturated vapor density. The y intercept (zero density) represents the second virial coefficient at a given temperature, and the third virial coefficient can be taken from the slope of each line at zero density. The values of the second virial coefficient calculated from the equation of state agree well with those determined numerically and shown as circles in the figure. Comparisons of second virial coefficients calculated with the equation of state and those determined from the data of de Vries (given in Table 9) are shown in Fig. 26. The uncertainty in the derived values at lower temperatures is higher due to the limited data at densities above 0.1 mol/dm^3 and to the higher curvature in the data.

5.3. Caloric Data

The sources of experimental data for the speed of sound of R-125 are summarized in Table 10 and shown graphically in Fig. 27. Comparisons of values calculated from the equation of state for the speed of sound are shown in Fig. 28 for the vapor phase and in Fig. 29 for the liquid phase. The equation represents the vapor phase data of Gillis (1997) and Ichikawa *et al.* (1998) within 0.01% and the liquid phase data of Takagi (1996) within 0.7%. There are no speed of sound data below 240 K; however, the extrapolation behavior of the equation of state is quite reasonable at low temperatures, as discussed below.

The reported measurements of the isochoric heat capacity, saturation liquid heat capacity, and isobaric heat capacity for R-125 are summarized in Table 11 and illustrated in Fig. 27. Comparisons of values calculated from the equation of state are shown for the isochoric heat capacities in Fig. 30, saturation liquid heat capacities in Fig. 31, and isobaric

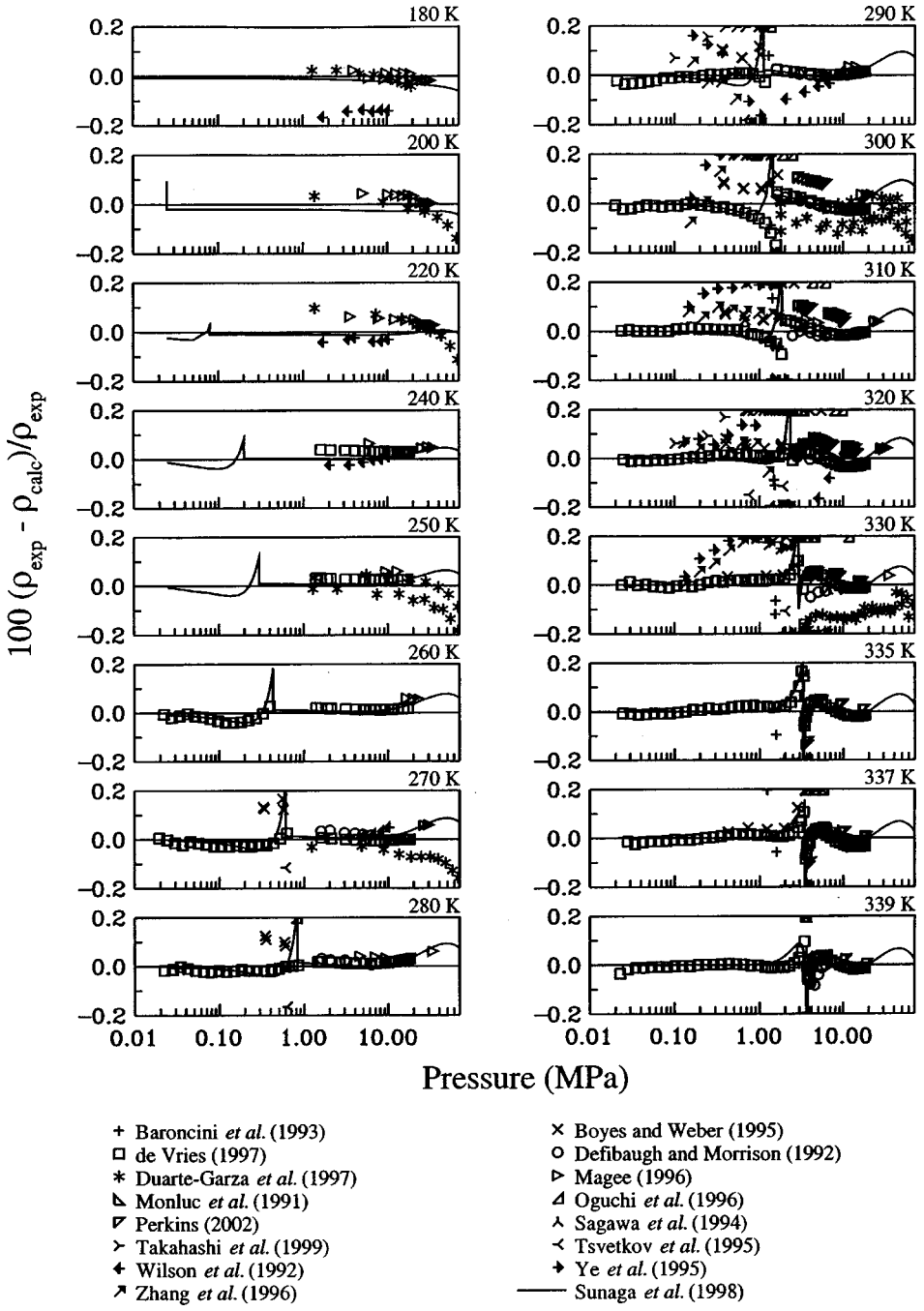

FIG. 23. Comparisons of densities calculated with the equation of state to experimental data.

heat capacities in Fig. 32. Lüddecke and Magee (1996) measured both the isochoric heat capacity of R-125 and the heat capacity along the saturated liquid line. The average deviation between values from the equation of state and these data is 0.57% for the isochoric heat capacity and 0.24% for the saturation liquid heat capacity. There are few experimental data for the isobaric heat capacity of R-125, especially in the vapor phase (five points by Wilson *et al.*, 1992), and the data in the liquid phase are not consistent. Although none of these data were used in the fit, the equation of state represents the data of Gunther and Steimle (1997) within 0.5%. This agreement indicates consistency between the fitted isochoric and saturation heat capacity data of Lüddecke and Magee and the isobaric heat capacity data of Gunther and Steimle.

5.4. Extrapolation Behavior

Plots of constant property lines on various thermodynamic coordinates are useful in assessing the behavior of the equation of state. The equation developed here was used to produce plots of temperature versus isochoric heat capacity (Fig.

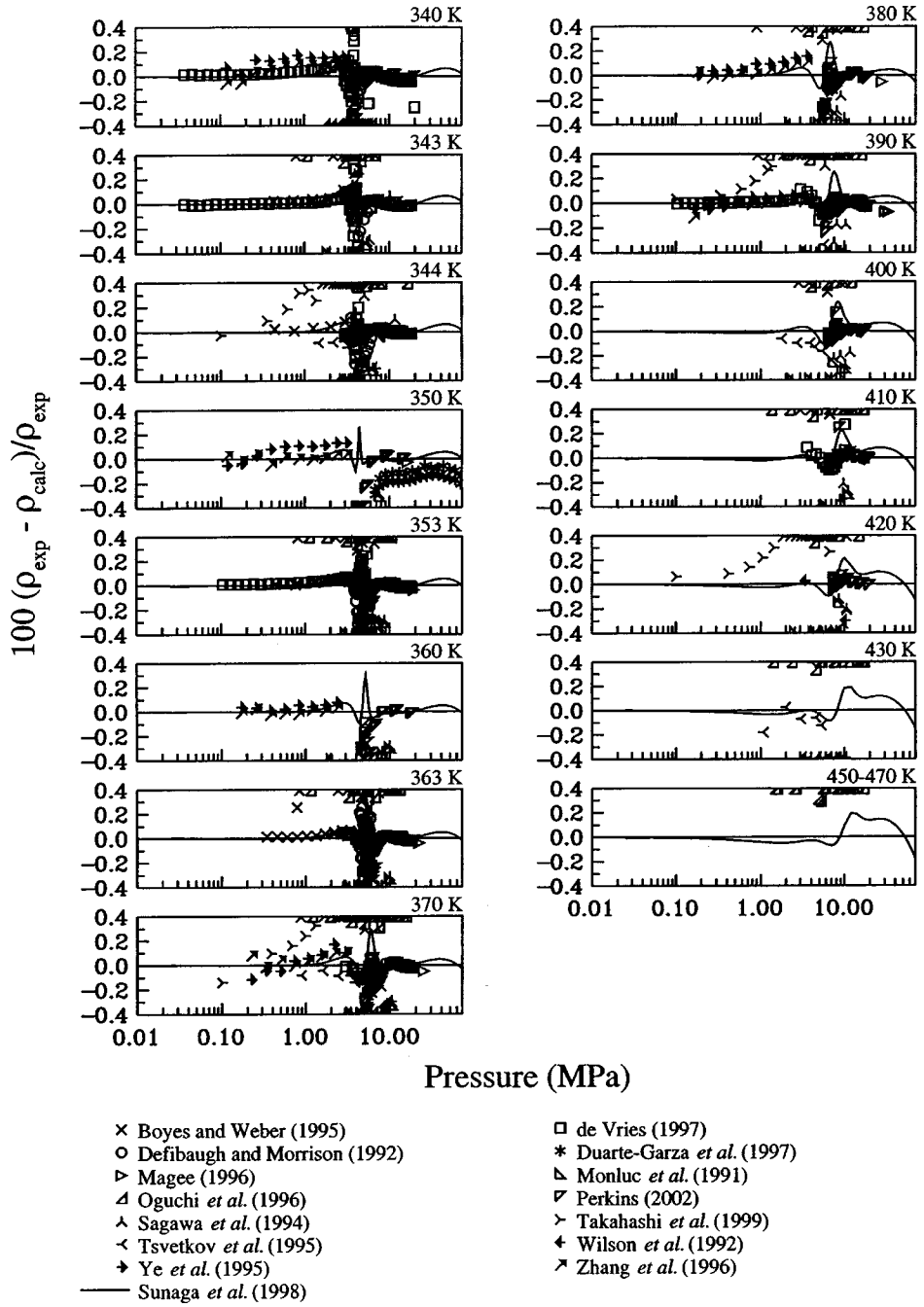

FIG. 23. (*Continued.*)

33), isobaric heat capacity (Fig. 34), and speed of sound (Fig. 35). These plots indicate that the equation of state exhibits reasonable behavior over all temperatures and pressures within the range of validity, and that the extrapolation behavior is reasonable at higher temperatures and pressures. Additional information about the extrapolation behavior was given earlier.

6. Estimated Uncertainties of Calculated Properties

The new reference equation of state for R-125 describes the $p\rho T$ surface with an uncertainty ($k=2$) of 0.1% in density at temperatures from the triple point to 400 K at pressures up to 60 MPa, except in the critical region, where an uncertainty of 0.2% in pressure is generally attained. In the limited region between 340 and 400 K and at pressures from 4 to 10 MPa, as well as for all states above 400 K, the uncertainty in density increases to 0.5%. At temperatures below 330 K and pressures below 30 MPa, the uncertainty in density in the liquid phase may be as low as 0.04%. In the vapor and supercritical region, speed of sound data are represented within 0.05% at pressures below 1 MPa. The estimated uncertainty for heat capacities is 0.5% and the estimated uncertainty for the speed of sound in the liquid phase

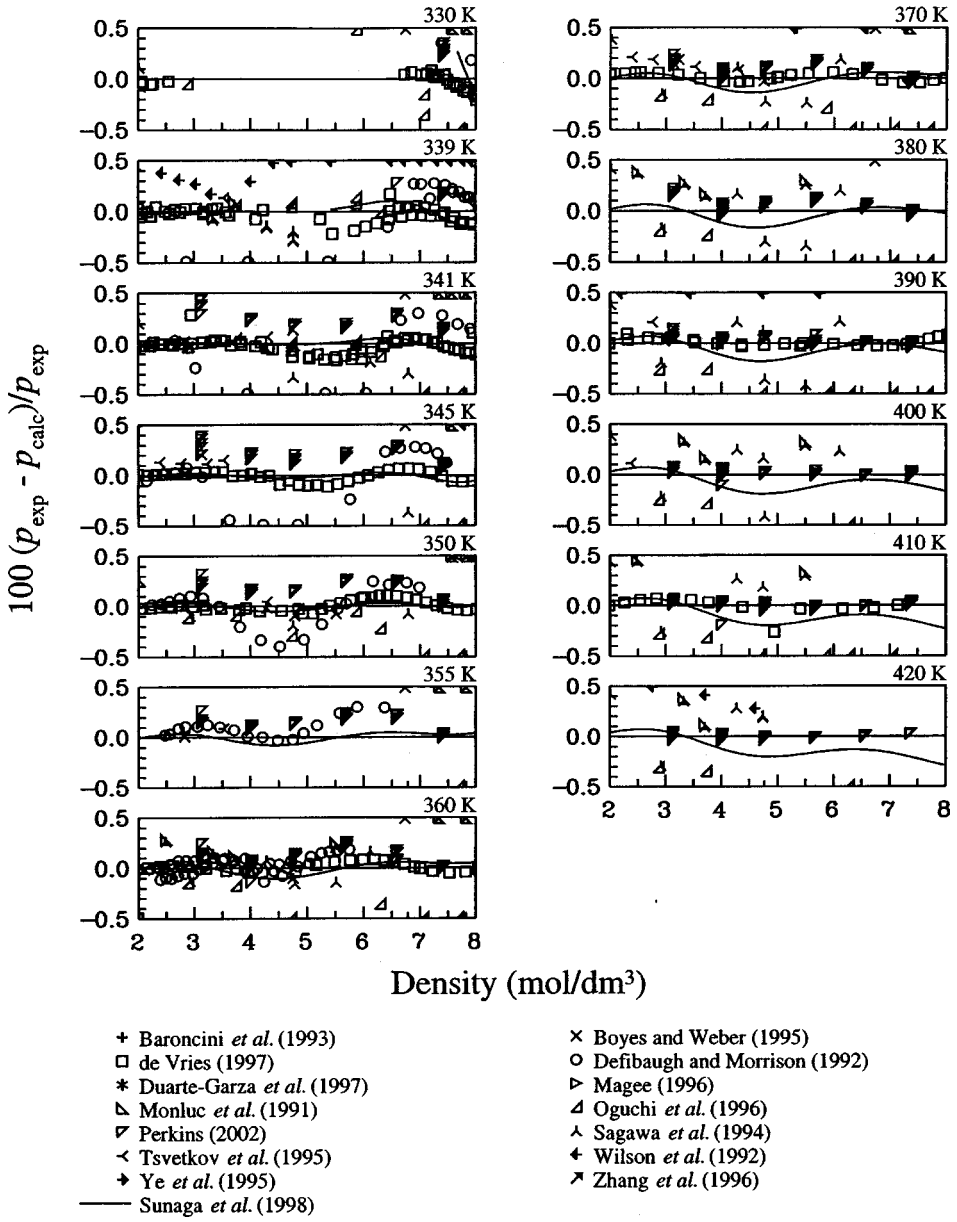

FIG. 24. Comparisons of pressures calculated with the equation of state to experimental data in the critical region.

TABLE 8. Summary of second virial coefficients

Author	No. of points	Temp. range (K)	AAD[a] (cm^3/mol)
Bignell and Dunlop (1993)	3	290–310	1.01
Boyes and Weber (1995)	8	280–350	2.34
de Vries (1997)[b]	19	263–413	1.44
Di Nicola *et al.* (2002)	10	303–363	1.23
Gillis (1997)	9	240–400	1.91
Grigiante *et al.* (2000)	7	260–360	0.93
Ye *et al.* (1995)	11	290–390	6.40
Zhang *et al.* (1995)	11	290–390	2.60

[a]Average absolute difference in the second virial coefficient (cm^3/mol).
[b]Data were derived from the $p\rho T$ data of de Vries and are given in Table 9.

is 0.5% for $T>250$ K. The saturation values can be calculated from the equation of state by application of the Maxwell criterion, which requires equal Gibbs energies and equal pressures for saturated liquid and vapor states at the same temperature. The estimated uncertainties of vapor pressures and saturated liquid densities calculated using the Maxwell criterion are 0.1% for each property, and the estimated uncertainty for saturated vapor densities is 0.2%. The uncertainty in density increases as the critical point is approached, while the accompanying uncertainty in calculated pressures is 0.2%. As an aid for computer implementation, calculated values of properties from the equation of state for R-125 are given in Table 12. The number of digits displayed does not indicate the accuracy in the values but is given for validation of computer code.

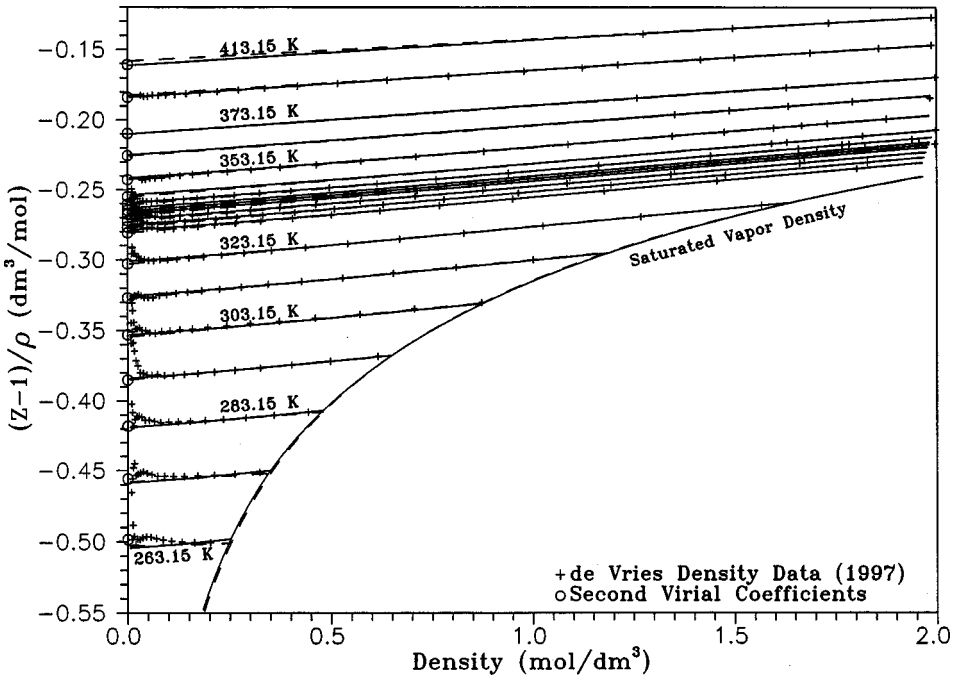

FIG. 25. Derivation of second virial coefficients from the $p\rho T$ data of de Vries (1997).

TABLE 9. Second virial coefficients derived from the $p\rho T$ data of de Vries (1997)

Temp. (K)	B (dm^3/mol)	Temp. (K)	B (dm^3/mol)
263.150	−0.4984	339.152	−0.2677
273.150	−0.4560	340.150	−0.2672
283.151	−0.4180	341.153	−0.2648
293.151	−0.3850	343.152	−0.2603
303.150	−0.3529	346.152	−0.2548
313.150	−0.3269	353.150	−0.2426
323.150	−0.3028	363.152	−0.2254
333.150	−0.2808	373.152	−0.2095
335.150	−0.2766	393.150	−0.1837
337.151	−0.2722	413.152	−0.1603

7. Acknowledgments

This work was funded by the 21-CR research program of the Air-Conditioning and Refrigeration Technology Institute; the Office of Building Technology, State and Community Programs of the U.S. Department of Energy. We thank Dr. Mark McLinden of NIST, Boulder, for his assistance and suggestions during the development and documentation of the equation. We are also grateful to Dr. Roland Span whose insights and collaborations have inspired us in various projects, including this one, over many years.

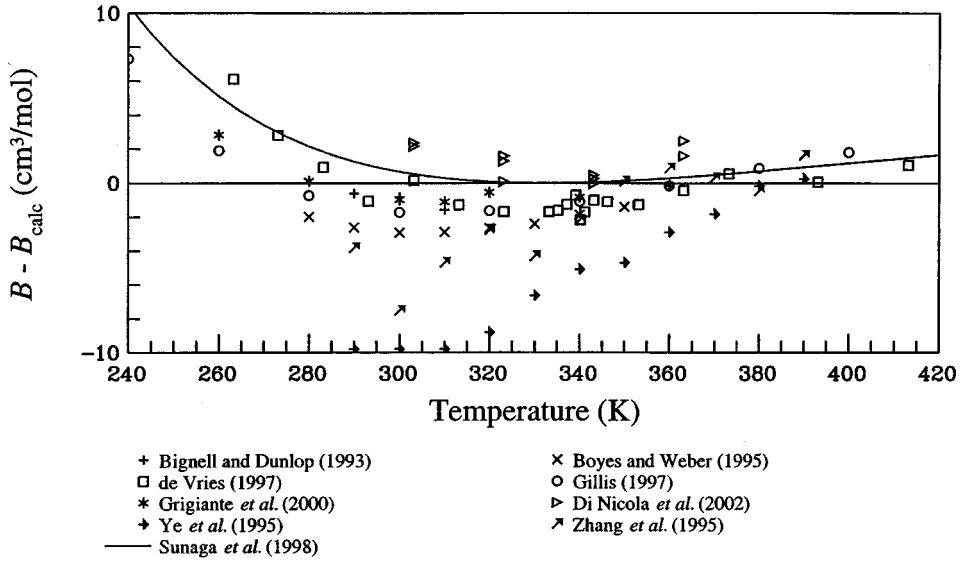

FIG. 26. Comparisons of second virial coefficients calculated with the equation of state to experimental data.

TABLE 10. Summary of speed of sound data

Author	No. of points	Temp. range (K)	Pressure range (MPa)	AAD (%)
Vapor Phase Data				
Hozumi *et al.* (1996)	72	273–343	0.01–0.24	0.034
Ichikawa *et al.* (1998)	74	273–343	0.01–0.50	0.007
Grigiante *et al.* (2000)	69	260–360	0.05–0.50	0.019
Gillis (1997)	149	240–400	0.04–1.02	0.008
Liquid Phase and Saturation Data				
Grebenkov *et al.* (1994)	30	288–333	1.14–16.4	0.233
Kraft and Leipertz (1994)	13	293–338	Sat. liq.	2.211
Kraft and Leipertz (1994)	9	307–338	Sat. vap.	1.560
Takagi (1996)	167	241–333	0.23–32.2	0.264

8. Appendix A: Thermodynamic Equations

The functional form of the Helmholtz energy equation of state is explicit in the dimensionless Helmholtz energy, α, using independent variables of dimensionless density and temperature,

$$\alpha(\delta,\tau)=\alpha^0(\delta,\tau)+\alpha^r(\delta,\tau), \tag{40}$$

where $\delta=\rho/\rho_c$ and $\tau=T_c/T$. The ideal gas Helmholtz energy is

$$\alpha^0=\ln\delta-\ln\tau+\sum_{k=1}^{3}a_k\tau^{t_k}+\sum_{k=4}^{6}a_k\ln[1-\exp(-b_k\tau)], \tag{41}$$

and the residual fluid Helmholtz energy is

$$\alpha^r(\delta,\tau)=\sum_{k=1}^{5}N_k\delta^{d_k}\tau^{t_k}+\sum_{k=6}^{15}N_k\delta^{d_k}\tau^{t_k}\exp(-\delta^{l_k})+\sum_{k=16}^{18}N_k\delta^{d_k}\tau^{t_k}\exp(-\delta^{l_k})\exp(-\tau^{m_k}). \tag{42}$$

The functions used for calculating pressure (p), compressibility factor (Z), internal energy (u), enthalpy (h), entropy (s), Gibbs energy (g), isochoric heat capacity (c_v), isobaric heat capacity (c_p), and the speed of sound (w) from Eq. (3) are given below.

$$p=\rho RT\left[1+\delta\left(\frac{\partial\alpha^r}{\partial\delta}\right)_\tau\right] \tag{43}$$

$$Z=\frac{p}{\rho RT}=1+\delta\left(\frac{\partial\alpha^r}{\partial\delta}\right)_\tau \tag{44}$$

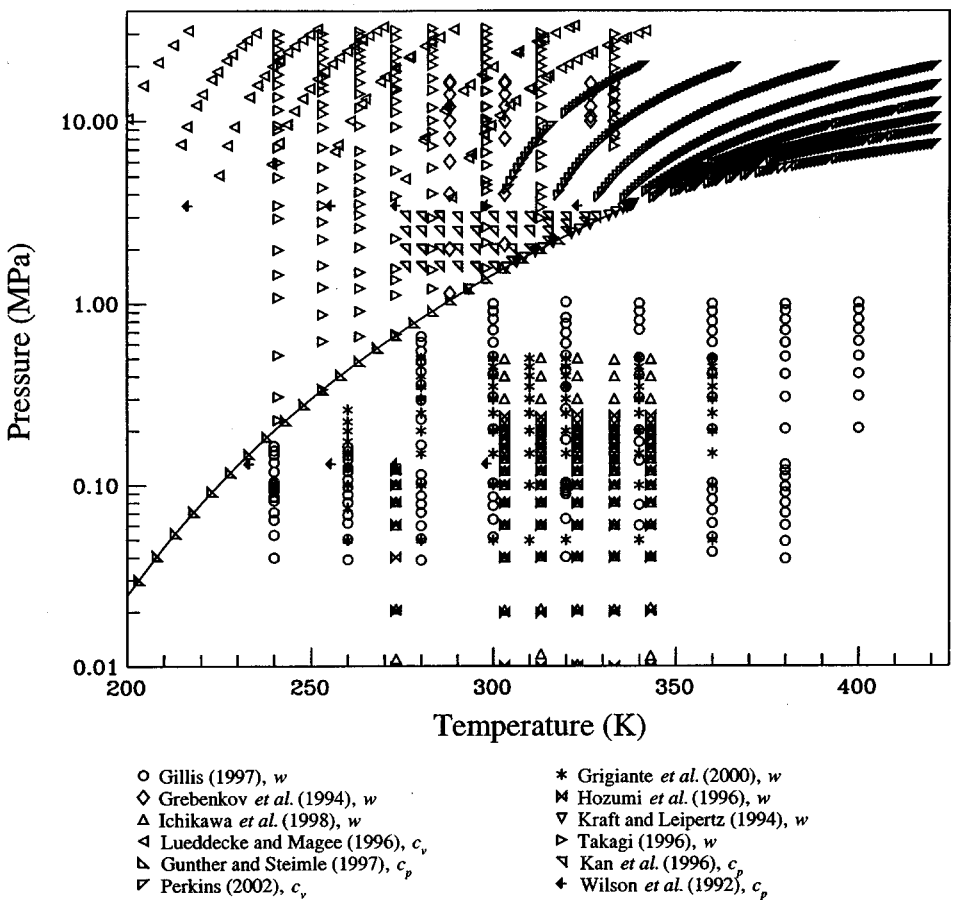

FIG. 27. Experimental isobaric and isochoric heat capacities and speed of sound data.

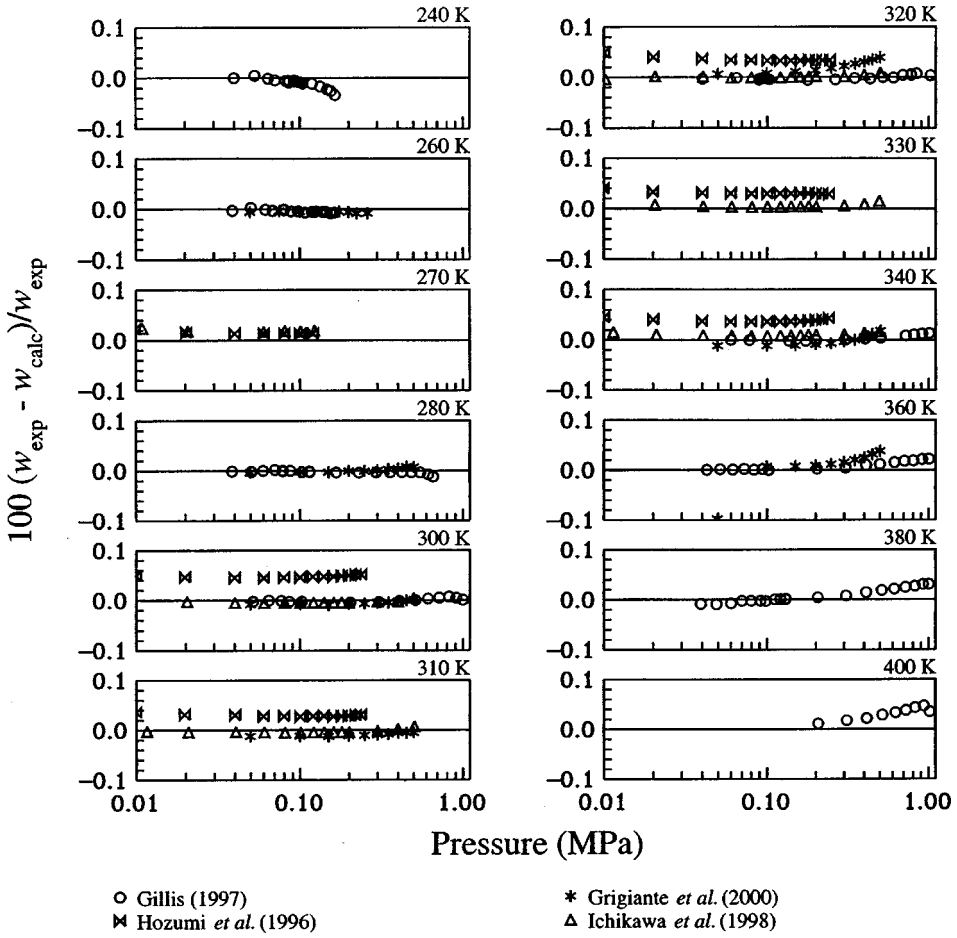

FIG. 28. Comparisons of speeds of sound in the vapor phase calculated with the equation of state to experimental data.

$$\frac{u}{RT}=\tau\left[\left(\frac{\partial\alpha^0}{\partial\tau}\right)_\delta+\left(\frac{\partial\alpha^r}{\partial\tau}\right)_\delta\right] \tag{45}$$

$$\frac{h}{RT}=\tau\left[\left(\frac{\partial\alpha^0}{\partial\tau}\right)_\delta+\left(\frac{\partial\alpha^r}{\partial\tau}\right)_\delta\right]+\delta\left(\frac{\partial\alpha^r}{\partial\delta}\right)_\tau+1 \tag{46}$$

$$\frac{s}{R}=\tau\left[\left(\frac{\partial\alpha^0}{\partial\tau}\right)_\delta+\left(\frac{\partial\alpha^r}{\partial\tau}\right)_\delta\right]-\alpha^0-\alpha^r \tag{47}$$

$$\frac{g}{RT}=1+\alpha^0+\alpha^r+\delta\left(\frac{\partial\alpha^r}{\partial\delta}\right)_\tau \tag{48}$$

$$\frac{c_v}{R}=-\tau^2\left[\left(\frac{\partial^2\alpha^0}{\partial\tau^2}\right)_\delta+\left(\frac{\partial^2\alpha^r}{\partial\tau^2}\right)_\delta\right] \tag{49}$$

$$\frac{c_p}{R}=\frac{c_v}{R}+\frac{\left[1+\delta\left(\frac{\partial\alpha^r}{\partial\delta}\right)_\tau-\delta\tau\left(\frac{\partial^2\alpha^r}{\partial\delta\partial\tau}\right)\right]^2}{\left[1+2\delta\left(\frac{\partial\alpha^r}{\partial\delta}\right)_\tau+\delta^2\left(\frac{\partial^2\alpha^r}{\partial\delta^2}\right)_\tau\right]} \tag{50}$$

$$\frac{w^2M}{RT}=1+2\delta\left(\frac{\partial\alpha^r}{\partial\delta}\right)_\tau+\delta^2\left(\frac{\partial^2\alpha^r}{\partial\delta^2}\right)_\tau-\frac{\left[1+\delta\left(\frac{\partial\alpha^r}{\partial\delta}\right)_\tau-\delta\tau\left(\frac{\partial^2\alpha^r}{\partial\delta\partial\tau}\right)\right]^2}{\tau^2\left[\left(\frac{\partial^2\alpha^0}{\partial\tau^2}\right)_\delta+\left(\frac{\partial^2\alpha^r}{\partial\tau^2}\right)_\delta\right]} \tag{51}$$

The fugacity coefficient and second and third virial coefficients are given by Eqs. (52)–(54).

$$\phi=\exp[Z-1-\ln(Z)+\alpha^r] \tag{52}$$

$$B(T)=\lim_{\delta\to0}\left[\frac{1}{\rho_c}\left(\frac{\partial\alpha^r}{\partial\delta}\right)\right] \tag{53}$$

$$C(T)=\lim_{\delta\to0}\left[\frac{1}{\rho_c^2}\left(\frac{\partial^2\alpha^r}{\partial\delta^2}\right)\right] \tag{54}$$

Other derived properties, given in Eqs. (55)–(57), include the first derivative of pressure with respect to density at constant temperature $(\partial p/\partial\rho)_T$, the second derivative of pressure with respect to density at constant temperature

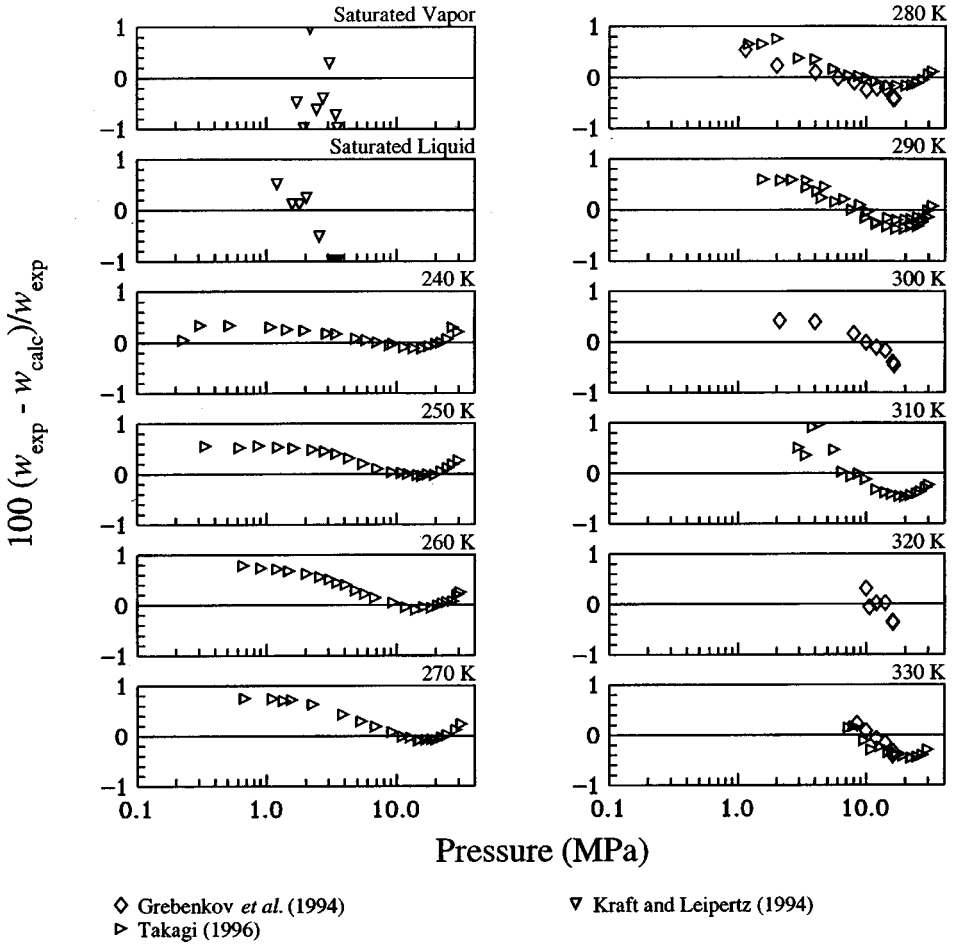

FIG. 29. Comparisons of speeds of sound in the liquid phase calculated with the equation of state to experimental data.

$(\partial^2 p/\partial\rho^2)_T$, and the first derivative of pressure with respect to temperature at constant density $(\partial p/\partial T)_\rho$.

$$\left(\frac{\partial p}{\partial \rho}\right)_T = RT\left[1 + 2\delta\left(\frac{\partial \alpha^r}{\partial \delta}\right)_\tau + \delta^2\left(\frac{\partial^2 \alpha^r}{\partial \delta^2}\right)_\tau\right] \quad (55)$$

$$\left(\frac{\partial^2 p}{\partial \rho^2}\right)_T = \frac{RT}{\rho}\left[2\delta\left(\frac{\partial \alpha^r}{\partial \delta}\right)_\tau + 4\delta^2\left(\frac{\partial^2 \alpha^r}{\partial \delta^2}\right)_\tau + \delta^3\left(\frac{\partial^3 \alpha^r}{\partial \delta^3}\right)_\tau\right] \quad (56)$$

$$\left(\frac{\partial p}{\partial T}\right)_\rho = R\rho\left[1 + \delta\left(\frac{\partial \alpha^r}{\partial \delta}\right)_\tau - \delta\tau\left(\frac{\partial^2 \alpha^r}{\partial \delta \partial \tau}\right)\right] \quad (57)$$

Equations for additional thermodynamic properties such as the isothermal compressibility and the Joule–Thomson coefficient are given in Lemmon *et al.* (2000).

The derivatives of the ideal gas Helmholtz energy required by the equations for the thermodynamic properties are

TABLE 11. Summary of experimental heat capacity data

Author	No. of points	Temp. range (K)	Density range (mol/dm^3)	Pressure range (MPa)	AAD (%)
Isochoric Heat Capacity Data					
Perkins (2002)	474	305–397		4.00–19.5	1.185
Lüddecke and Magee (1996)	99	200–342	10.5–13.5		0.577
Saturation Heat Capacity Data					
Lüddecke and Magee (1996)	93	176–278			0.244
Isobaric Heat Capacity Data					
Kan *et al.* (1996)	78	276–328		1.59–3.04	1.820
Wilson *et al.* (1992)	10	216–333		0.13–3.45	1.182
Gunther and Steimle (1997)	24	203–318		Sat. liq.	0.520

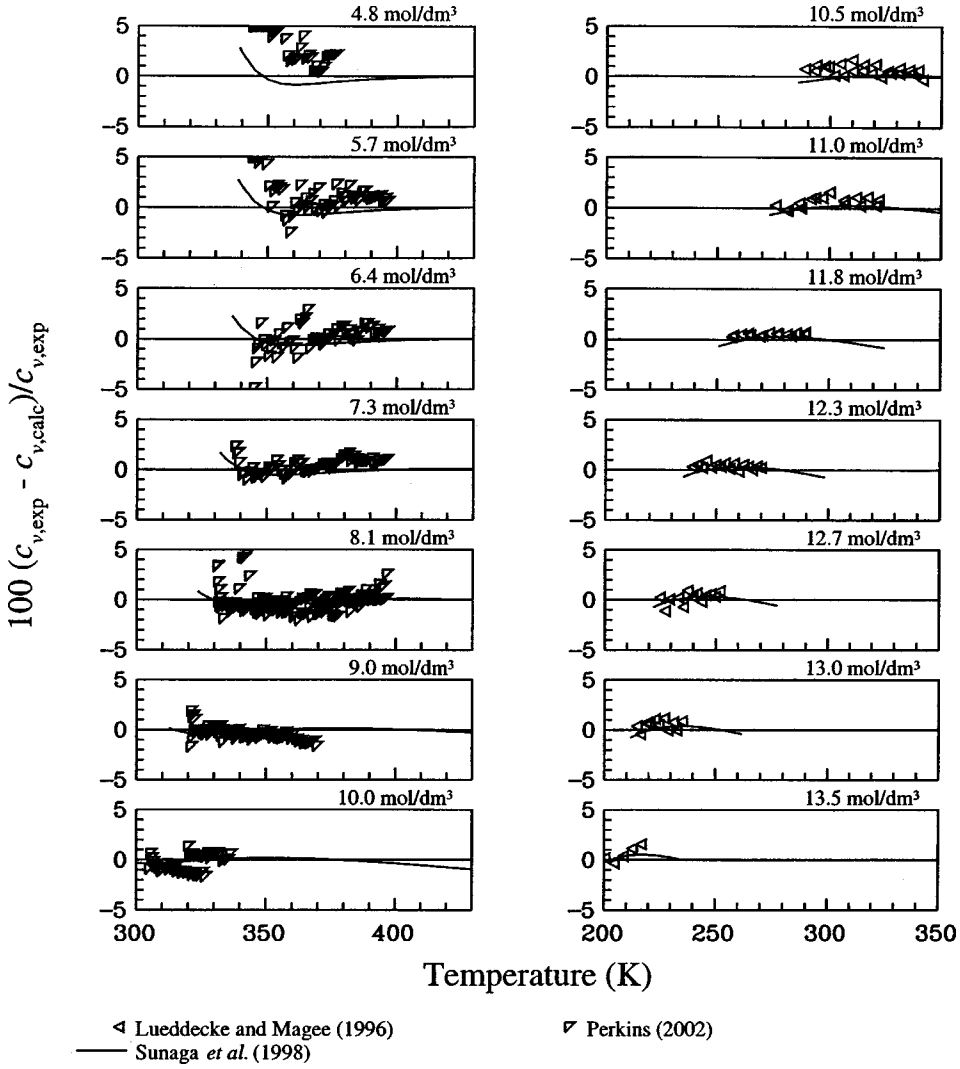

FIG. 30. Comparisons of isochoric heat capacities calculated with the equation of state to experimental data.

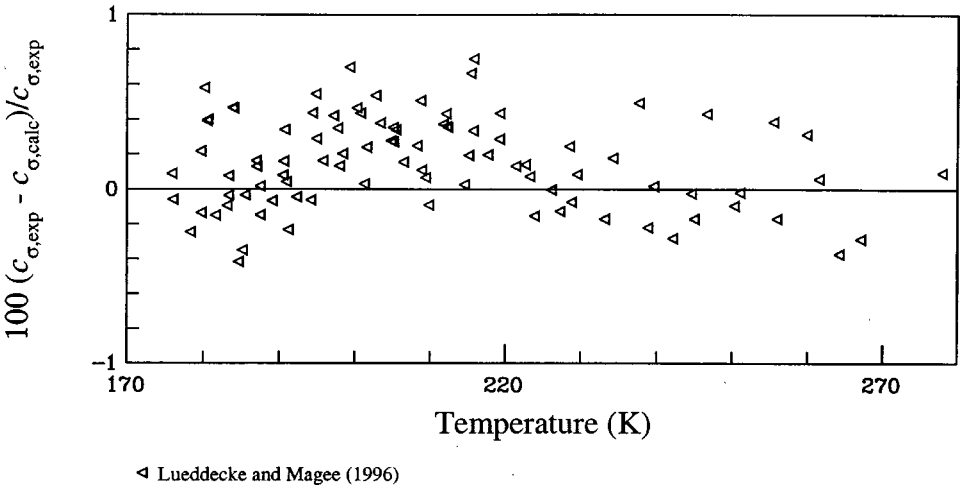

FIG. 31. Comparisons of saturation heat capacities calculated with the equation of state to experimental data.

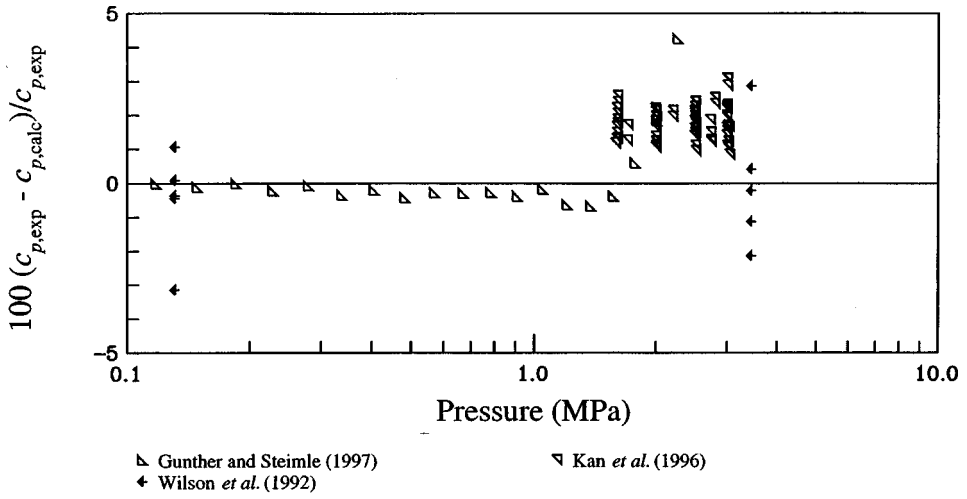

FIG. 32. Comparisons of isobaric heat capacities calculated with the equation of state to experimental data.

$$\tau\frac{\partial\alpha^0}{\partial\tau}=-1+\sum_{k=1}^{3}t_k a_k\tau^{t_k}+\tau\sum_{k=4}^{6}a_k b_k\left[\frac{1}{\exp(b_k\tau)-1}\right], \tag{58}$$

and

$$\tau^2\frac{\partial^2\alpha^0}{\partial\tau^2}=1+\sum_{k=1}^{3}t_k(t_k-1)a_k\tau^{t_k}-\tau^2\sum_{k=4}^{6}a_k b_k^2\frac{\exp(b_k\tau)}{[\exp(b_k\tau)-1]^2}. \tag{59}$$

The derivatives of the residual Helmholtz energy are given in Eqs. (60)–(65).

$$\delta\frac{\partial\alpha^r}{\partial\delta}=\sum_{k=1}^{5}d_k N_k\delta^{d_k}\tau^{t_k}+\sum_{k=6}^{15}N_k\delta^{d_k}\tau^{t_k}\exp(-\delta^{l_k})\times(d_k-l_k\delta^{l_k})+\sum_{k=16}^{18}N_k\delta^{d_k}\tau^{t_k}\exp(-\delta^{l_k})\times\exp(-\tau^{m_k})(d_k-l_k\delta^{l_k}) \tag{60}$$

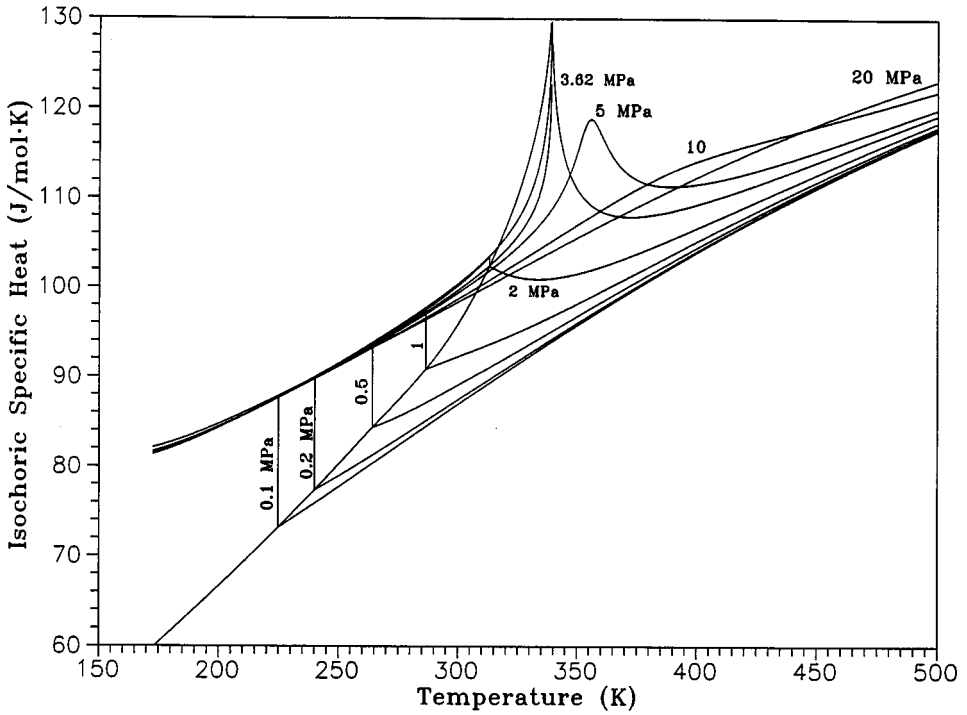

FIG. 33. Isochoric heat capacity versus temperature diagram.

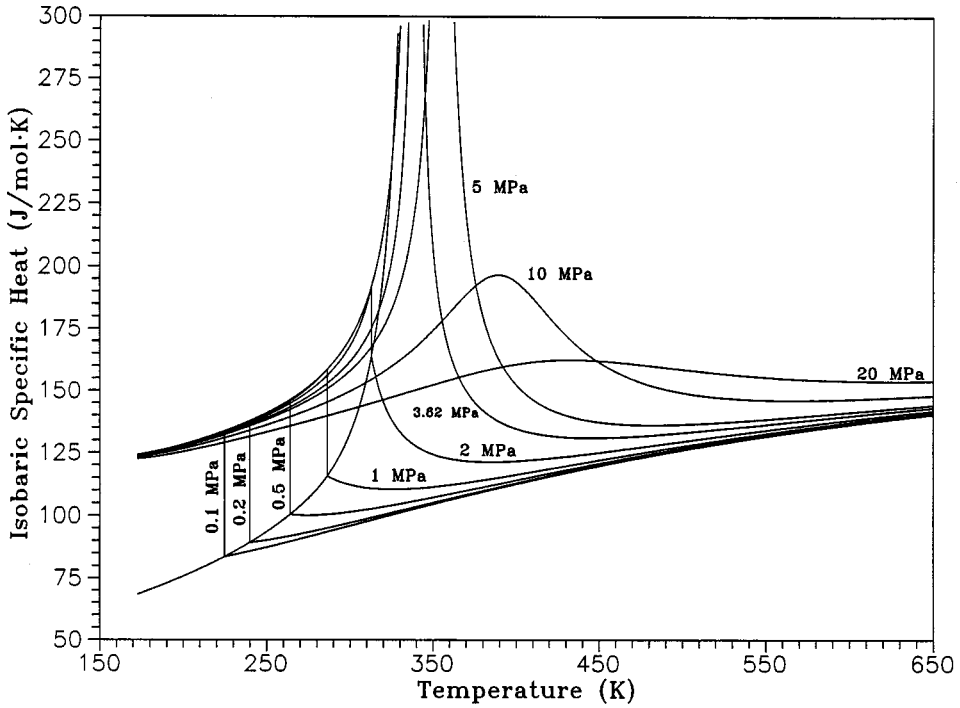

FIG. 34. Isobaric heat capacity versus temperature diagram.

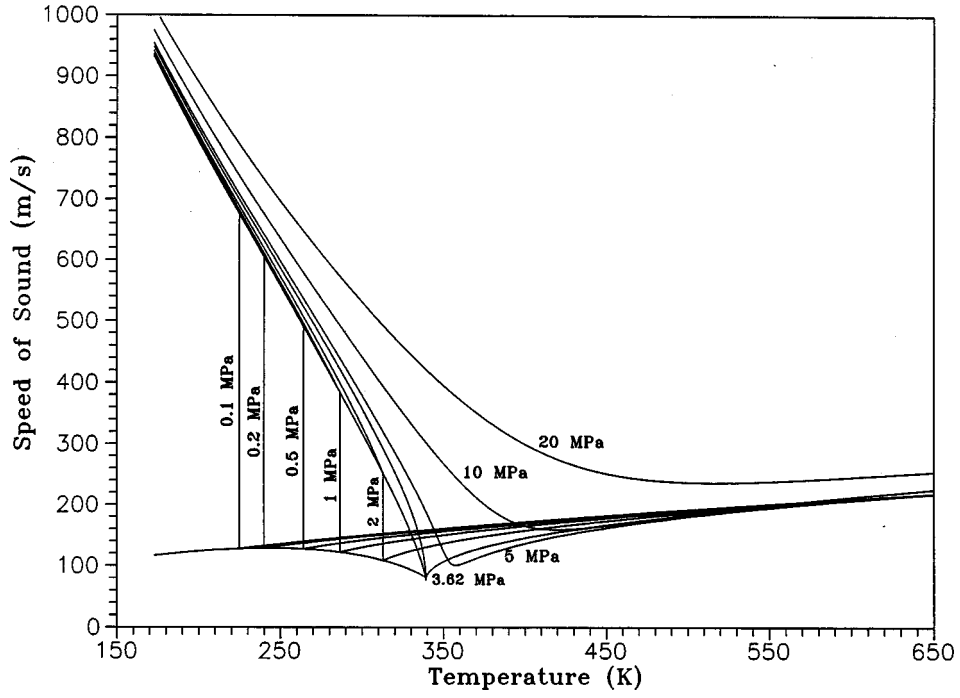

FIG. 35. Speed of sound versus temperature diagram.

TABLE 12. Calculated values of properties for algorithm verification

Temperature (K)	Density (mol/dm^3)	Pressure (MPa)	Isochoric heat capacity (J/mol·K)	Isobaric heat capacity (J/mol·K)	Speed of sound (m/s)
200.0	14.0	42.302 520	85.816 305	123.536 41	968.671 94
300.0	10.0	2.902 3498	99.919 660	164.169 14	345.912 35
300.0	0.7	1.324 5058	94.823 171	124.960 09	120.560 07
400.0	5.0	9.049 5658	114.418 19	198.117 92	151.530 60
339.2	4.8	3.620 1215	130.636 50	274 863.02	78.735 928

$$\delta^2\frac{\partial^2\alpha^r}{\partial\delta^2}=\sum_{k=1}^{5} d_k(d_k-1)N_k\delta^{d_k}\tau^{t_k}+\sum_{k=6}^{15} N_k\delta^{d_k}\tau^{t_k}\exp(-\delta^{l_k})\times[(d_k-l_k\delta^{l_k})(d_k-1-l_k\delta^{l_k})-l_k^2\delta^{l_k}]+\sum_{k=16}^{18} N_k\delta^{d_k}\tau^{t_k}\exp(-\delta^{l_k})\exp(-\tau^{m_k})\times[(d_k-l_k\delta^{l_k})(d_k-1-l_k\delta^{l_k})-l_k^2\delta^{l_k}] \quad (61)$$

$$\delta^3\frac{\partial^3\alpha^r}{\partial\delta^3}=\sum_{k=1}^{5} d_k(d_k-1)(d_k-2)N_k\delta^{d_k}\tau^{t_k}+\sum_{k=6}^{15} N_k\delta^{d_k}\tau^{t_k}\exp(-\delta^{l_k})\{d_k(d_k-1)(d_k-2)+\delta^{l_k}[-2l_k+6d_kl_k-3d_k^2l_k-3d_kl_k^2+3l_k^2-l_k^3]+\delta^{2l_k}[3d_kl_k^2-3l_k^2+3l_k^3]-l_k^3\delta^{3l_k}\}+\sum_{k=16}^{18} N_k\delta^{d_k}\tau^{t_k}\exp(-\delta^{l_k})\exp(-\tau^{m_k})\times\{d_k(d_k-1)(d_k-2)+\delta^{l_k}[-2l_k+6d_kl_k-3d_k^2l_k-3d_kl_k^2+3l_k^2-l_k^3]+\delta^{2l_k}[3d_kl_k^2-3l_k^2+3l_k^3]-l_k^3\delta^{3l_k}\} \quad (62)$$

$$\tau\frac{\partial\alpha^r}{\partial\tau}=\sum_{k=1}^{5} t_kN_k\delta^{d_k}\tau^{t_k}+\sum_{k=6}^{15} t_kN_k\delta^{d_k}\tau^{t_k}\exp(-\delta^{l_k})+\sum_{k=16}^{18} N_k\delta^{d_k}\tau^{t_k}\exp(-\delta^{l_k})\exp(-\tau^{m_k})\times(t_k-m_k\tau^{m_k}) \quad (63)$$

$$\tau^2\frac{\partial^2\alpha^r}{\partial\tau^2}=\sum_{k=1}^{5} t_k(t_k-1)N_k\delta^{d_k}\tau^{t_k}+\sum_{k=6}^{15} t_k(t_k-1)N_k\delta^{d_k}\tau^{t_k}\times\exp(-\delta^{l_k})+\sum_{k=16}^{18} N_k\delta^{d_k}\tau^{t_k}\exp(-\delta^{l_k})\times\exp(-\tau^{m_k})[(t_k-m_k\tau^{m_k})(t_k-1-m_k\tau^{m_k})-m_k^2\tau^{m_k}] \quad (64)$$

$$\tau\delta\frac{\partial^2\alpha^r}{\partial\tau\partial\delta}=\sum_{k=1}^{5} d_kt_kN_k\delta^{d_k}\tau^{t_k}+\sum_{k=6}^{15} t_kN_k\delta^{d_k}\tau^{t_k}\exp(-\delta^{l_k})\times(d_k-l_k\delta^{l_k})+\sum_{k=16}^{18} N_k\delta^{d_k}\tau^{t_k}\exp(-\delta^{l_k})\times\exp(-\tau^{m_k})(d_k-l_k\delta^{l_k})(t_k-m_k\tau^{m_k}) \quad (65)$$

9. Appendix B: Tables of Thermodynamic Properties of R-125 at Saturation

T (°C)	p (MPa)	ρ (kg/m^3)	h (kJ/kg)	s (kJ/(kg K))	c_v (kJ/(kg K))	c_p (kJ/(kg K))	w (m/s)
−100.630	0.002 91	1690.7	87.130	.490 22	0.6776	1.035	932.6
		0.244 62	277.39	1.5931	0.4984	0.5689	116.4
−100.	0.003 09	1688.7	87.782	.493 99	0.6781	1.035	929.2
		0.258 34	277.74	1.5911	0.4997	0.5703	116.6
−95.	0.004 81	1672.5	92.969	.523 52	0.6818	1.040	903.2
		0.391 79	280.54	1.5764	0.5099	0.5810	118.0
−90.	0.007 29	1656.2	98.181	.552 36	0.6860	1.045	877.5
		0.577 94	283.36	1.5634	0.5201	0.5919	119.4
−85.	0.010 74	1639.9	103.42	.580 59	0.6906	1.051	852.3
		0.831 42	286.20	1.5520	0.5304	0.6031	120.7
−80.	0.015 47	1623.4	108.70	.608 24	0.6955	1.058	827.5
		1.1691	289.06	1.5421	0.5409	0.6146	121.9

T (°C)	p (MPa)	ρ (kg/m^3)	h (kJ/kg)	s (kJ/(kg K))	c_v (kJ/(kg K))	c_p (kJ/(kg K))	w (m/s)
−75.	0.021 79	1606.7	114.01	.635 37	0.7006	1.066	802.9
		1.6103	291.94	1.5333	0.5514	0.6264	123.1
−70.	0.030 08	1589.9	119.36	.662 01	0.7060	1.074	778.6
		2.1766	294.83	1.5257	0.5620	0.6385	124.1
−65.	0.040 76	1572.9	124.75	.688 21	0.7115	1.082	754.5
		2.8921	297.71	1.5191	0.5727	0.6511	125.1
−60.	0.054 32	1555.7	130.19	.713 98	0.7171	1.091	730.6
		3.7833	300.60	1.5135	0.5836	0.6641	126.0
−55.	0.071 26	1538.2	135.68	.739 37	0.7229	1.101	706.8
		4.8791	303.48	1.5086	0.5946	0.6776	126.8
−50.	0.092 16	1520.5	141.21	.764 39	0.7288	1.111	683.2
		6.2112	306.35	1.5044	0.6058	0.6916	127.4
−45.	0.117 63	1502.4	146.80	.789 07	0.7349	1.121	659.6
		7.8140	309.20	1.5009	0.6171	0.7063	127.9
−40.	0.148 30	1484.0	152.44	.813 45	0.7410	1.132	636.1
		9.7249	312.03	1.4980	0.6286	0.7216	128.3
−35.	0.184 87	1465.3	158.14	.837 53	0.7473	1.144	612.6
		11.985	314.84	1.4955	0.6402	0.7376	128.6
−30.	0.228 06	1446.1	163.90	.861 35	0.7537	1.157	589.1
		14.639	317.61	1.4935	0.6520	0.7545	128.7
−25.	0.278 61	1426.5	169.73	.884 93	0.7602	1.170	565.7
		17.736	320.34	1.4919	0.6640	0.7724	128.7
−20.	0.337 33	1406.4	175.62	.908 29	0.7668	1.184	542.2
		21.331	323.03	1.4906	0.6761	0.7912	128.5
−15.	0.405 01	1385.8	181.59	.931 45	0.7736	1.199	518.7
		25.486	325.67	1.4895	0.6882	0.8112	128.1
−10.	0.482 52	1364.5	187.64	.954 43	0.7805	1.216	495.2
		30.271	328.24	1.4887	0.7003	0.8324	127.5
−5.	0.570 72	1342.6	193.77	.977 28	0.7876	1.234	471.6
		35.768	330.74	1.4881	0.7122	0.8550	126.8
0.	0.670 52	1319.8	200.00	1.0000	0.7948	1.255	448.0
		42.070	333.16	1.4875	0.7240	0.8797	125.8
5.	0.782 88	1296.2	206.33	1.0226	0.8021	1.277	424.3
		49.291	335.47	1.4869	0.7359	0.9073	124.6
10.	0.908 75	1271.5	212.76	1.0452	0.8095	1.303	400.4
		57.564	337.66	1.4863	0.7483	0.9392	123.2
15.	1.049 18	1245.6	219.32	1.0678	0.8172	1.332	376.3
		67.054	339.71	1.4856	0.7617	0.9770	121.5
20.	1.205 20	1218.3	226.02	1.0904	0.8252	1.367	352.0
		77.966	341.58	1.4846	0.7764	1.023	119.6
25.	1.377 92	1189.4	232.87	1.1131	0.8335	1.407	327.4
		90.557	343.26	1.4834	0.7928	1.080	117.3
30.	1.568 53	1158.4	239.91	1.1359	0.8425	1.457	302.4
		105.17	344.71	1.4817	0.8111	1.152	114.8
35.	1.778 27	1125.0	247.16	1.1591	0.8522	1.521	276.9
		122.27	345.88	1.4794	0.8315	1.245	111.9
40.	2.008 49	1088.4	254.67	1.1826	0.8630	1.605	250.8
		142.52	346.69	1.4764	0.8542	1.372	108.6
45.	2.260 74	1047.7	262.52	1.2067	0.8755	1.724	223.8
		166.95	347.05	1.4724	0.8796	1.553	104.8
50.	2.536 80	1001.1	270.83	1.2318	0.8907	1.910	195.6
		197.29	346.75	1.4667	0.9083	1.842	100.5
55.	2.838 91	945.35	279.83	1.2585	0.9106	2.252	165.3

T (°C)	p (MPa)	ρ (kg/m^3)	h (kJ/kg)	s (kJ/(kg K))	c_v (kJ/(kg K))	c_p (kJ/(kg K))	w (m/s)
		236.92	345.44	1.4584	0.9421	2.386	95.6
60.	3.170 28	872.09	290.10	1.2884	0.9411	3.139	131.5
		294.37	342.21	1.4448	0.9856	3.833	89.8
65.	3.536 97	735.11	304.88	1.3311	1.014	13.67	90.0
		416.57	332.24	1.4120	1.060	20.07	82.6
66.	3.616 07	612.97	314.86	1.3602	1.078	818.2	78.9
		534.59	321.41	1.3795	1.093	923.0	79.2
66.023	3.617 70	573.58	318.06	1.3696			
−100.630	0.002 91	1690.7	87.130	.490 22	0.6776	1.035	932.6
		0.244 62	277.39	1.5931	0.4984	0.5689	116.4
−76.278	0.02	1611.0	112.65	.628 49	0.6993	1.064	809.2
		1.4866	291.20	1.5355	0.5487	0.6233	122.8
−65.319	0.04	1574.0	124.41	.686 55	0.7111	1.082	756.1
		2.8415	297.53	1.5195	0.5721	0.6503	125.0
−58.200	0.06	1549.4	132.16	.723 16	0.7192	1.095	722.0
		4.1526	301.64	1.5116	0.5876	0.6689	126.3
−52.785	0.08	1530.4	138.12	.750 49	0.7255	1.105	696.3
		5.4381	304.75	1.5067	0.5996	0.6837	127.1
−48.356	0.10	1514.6	143.04	.772 54	0.7308	1.114	675.4
		6.7064	307.29	1.5032	0.6095	0.6964	127.6
−48.089	0.101 325	1513.6	143.34	.773 86	0.7311	1.115	674.2
		6.7900	307.44	1.5030	0.6101	0.6971	127.6
−39.747	0.15	1483.1	152.73	.814 67	0.7413	1.133	634.9
		9.8304	312.18	1.4978	0.6292	0.7224	128.4
−33.154	0.20	1458.3	160.26	.846 35	0.7496	1.149	603.9
		12.916	315.87	1.4947	0.6446	0.7438	128.7
−27.735	0.25	1437.3	166.53	.872 06	0.7566	1.162	578.5
		15.984	318.85	1.4927	0.6574	0.7625	128.7
−23.093	0.30	1418.9	171.97	.893 86	0.7627	1.175	556.7
		19.045	321.37	1.4913	0.6686	0.7795	128.6
−19.009	0.35	1402.4	176.80	.912 89	0.7681	1.187	537.6
		22.108	323.56	1.4904	0.6785	0.7951	128.4
−15.347	0.40	1387.3	181.18	.929 84	0.7731	1.198	520.4
		25.178	325.49	1.4896	0.6874	0.8098	128.1
−12.018	0.45	1373.2	185.19	.945 18	0.7777	1.209	504.7
		28.259	327.21	1.4890	0.6954	0.8237	127.8
−8.957	0.50	1360.0	188.91	.959 21	0.7820	1.220	490.3
		31.356	328.77	1.4886	0.7028	0.8370	127.4
−6.119	0.55	1347.6	192.39	.972 17	0.7860	1.230	476.9
		34.471	330.19	1.4882	0.7095	0.8498	127.0
−3.469	0.60	1335.7	195.67	.984 24	0.7898	1.240	464.4
		37.607	331.49	1.4879	0.7158	0.8623	126.5
−0.980	0.65	1324.3	198.77	.995 55	0.7933	1.251	452.6
		40.766	332.69	1.4876	0.7217	0.8747	126.0
1.369	0.70	1313.4	201.72	1.0062	0.7967	1.261	441.5
		43.951	333.80	1.4873	0.7272	0.8869	125.5
3.596	0.75	1302.9	204.54	1.0163	0.8000	1.271	431.0
		47.163	334.83	1.4871	0.7325	0.8992	125.0
5.714	0.80	1292.7	207.24	1.0259	0.8031	1.281	420.9
		50.404	335.79	1.4869	0.7377	0.9116	124.4
7.735	0.85	1282.8	209.83	1.0350	0.8061	1.291	411.2
		53.677	336.68	1.4866	0.7426	0.9242	123.8

T (°C)	p (MPa)	ρ (kg/m^3)	h (kJ/kg)	s (kJ/(kg K))	c_v (kJ/(kg K))	c_p (kJ/(kg K))	w (m/s)
9.670	0.90	1273.1	212.33	1.0437	0.8090	1.301	402.0
		56.982	337.52	1.4864	0.7475	0.9370	123.3
11.525	0.95	1263.7	214.75	1.0521	0.8118	1.311	393.1
		60.321	338.30	1.4861	0.7523	0.9500	122.7
13.309	1.00	1254.5	217.09	1.0602	0.8146	1.322	384.5
		63.697	339.03	1.4858	0.7570	0.9635	122.1
16.686	1.10	1236.6	221.56	1.0754	0.8198	1.343	368.1
		70.564	340.36	1.4853	0.7665	0.9915	120.9
19.841	1.20	1219.2	225.80	1.0897	0.8249	1.365	352.8
		77.596	341.53	1.4847	0.7759	1.021	119.6
22.806	1.30	1202.3	229.84	1.1031	0.8298	1.389	338.2
		84.806	342.55	1.4839	0.7854	1.053	118.3
25.605	1.40	1185.7	233.71	1.1158	0.8346	1.413	324.4
		92.209	343.45	1.4832	0.7949	1.088	117.0
28.258	1.50	1169.4	237.43	1.1280	0.8393	1.439	311.1
		99.823	344.24	1.4823	0.8045	1.125	115.7
30.781	1.60	1153.4	241.02	1.1395	0.8439	1.466	298.4
		107.66	344.91	1.4814	0.8141	1.165	114.3
33.189	1.70	1137.4	244.50	1.1507	0.8486	1.496	286.2
		115.75	345.49	1.4803	0.8238	1.208	113.0
35.492	1.80	1121.5	247.88	1.1614	0.8532	1.528	274.3
		124.11	345.98	1.4792	0.8336	1.256	111.6
39.823	2.00	1089.8	254.40	1.1817	0.8626	1.602	251.7
		141.74	346.67	1.4766	0.8534	1.366	108.7
43.837	2.20	1057.6	260.66	1.2010	0.8724	1.692	230.2
		160.82	347.01	1.4734	0.8734	1.504	105.7
47.578	2.40	1024.5	266.74	1.2195	0.8829	1.809	209.4
		181.71	346.99	1.4697	0.8939	1.684	102.7
51.084	2.60	989.96	272.71	1.2374	0.8945	1.966	189.2
		204.93	346.57	1.4652	0.9151	1.930	99.5
54.381	2.80	952.95	278.66	1.2550	0.9077	2.194	169.2
		231.31	345.68	1.4596	0.9375	2.294	96.2
57.490	3.00	912.04	284.72	1.2728	0.9237	2.565	149.1
		262.29	344.18	1.4526	0.9620	2.893	92.8
60.426	3.20	864.39	291.08	1.2912	0.9446	3.288	128.4
		300.75	341.78	1.4432	0.9901	4.077	89.3
63.198	3.40	802.42	298.28	1.3120	0.9757	5.402	106.5
		354.37	337.68	1.4292	1.02	7.502	85.6
65.800	3.60	668.27	310.49	1.3474	1.052	71.10	81.4
		480.94	326.28	1.3940	1.085	95.87	80.5
66.023	3.6177	573.58	318.06	1.3696			

10. References

Angus, S., B. Armstrong, and K. M. de Reuck, *International Thermodynamic Tables of the Fluid State-7 Propylene*, *International Union of Pure and Applied Chemistry* (Pergamon Press, Oxford, 1980).

Baroncini, C., G. Giuliani, and F. Polonara, 3rd World Conf. on Experimental Heat Transfer, Fluid Mechanics and Thermodynamics, Vol. 2, 1993, p. 1774.

Bignell, C. M. and P. J. Dunlop, J. Chem. Phys. **98**, 4889 (1993).

Boyes, S. J. and L. A. Weber, J. Chem. Thermodyn. **27**, 163 (1995).

Bücker, D. and W. Wagner, J. Phys. Chem. Ref. Data (in press, 2004).

Chen, S. S., A. S. Rodgers, J. Chao, R. C. Wilhoit, and B. J. Zwolinski, J. Phys. Chem. Ref. Data **4**, 441 (1975).

Defibaugh, D. R. and G. Morrison, Fluid Phase Equilib. **80**, 157 (1992).

Deiters, U. K. and K. M. de Reuck, Pure Appl. Chem. **69**, 1237 (1997).

de Reuck, K. M., *International Thermodynamic Tables of the Fluid State-11 Fluorine*, *International Union of Pure and Applied Chemistry* (Pergamon Press, Oxford, 1990).

de Reuck, K. M. and R. J. B. Craven, *International Thermodynamic Tables of the Fluid State-12 Methanol*, *International Union of Pure and Applied Chemistry* (Blackwell Scientific Publications, London, 1993).

de Reuck, K. M., R. J. B. Craven, and W. A. Cole, Report on the Development of an Equation of State for Sulphur Hexafluoride, IUPAC Thermodynamic Tables Project Centre, London, 1991.

de Vries, B., Thermodynamische Eigenschaften der Alternativen Kaeltemittel R32, R125 und R143a—Messungen und Zustandsgleichungen, Dissertation, University of Hannover, Germany, 1997.

de Vries, B., R. Tillner-Roth, and H. D. Baehr, 19th International Congress of Refrigeration, The Hague, The Netherlands, International Institute of Refrigeration, Vol. IVa, 1995, p. 582.
Di Nicola, G., G. Giuliani, F. Polonara, R. Stryjek, Fluid Phase Equilib. **199**, 161 (2002).
Duarte-Garza, H. A. and J. W. Magee, Int. J. Thermophys. **18**, 173 (1997).
Duarte-Garza, H. A., C. E. Stouffer, K. R. Hall, J. C. Holste, K. N. Marsh, and B. E. Gammon, J. Chem. Eng. Data **42**, 745 (1997).
Elhassan, A. E., R. J. B. Craven, and K. M. de Reuck, Fluid Phase Equilib. **130**, 167 (1997).
Ely, J. F., Colorado School of Mines, Golden, Colorado (private communication, 1995).
Fukushima, M. and S. Ohotoshi, 13th Japan Symp. Thermophys. Prop., 1992, p. 49.
Gillis, K. A., Int. J. Thermophys. **18**, 73 (1997).
Gorenflo, D., R. Koester, and G. Herres, Universität Paderborn, Germany (private communication, 1996).
Grebenkov, A. J., Yu. G. Kotelevsky, V. V. Saplitza, O. V. Beljaeva, T. A. Zajatz, and B. D. Timofeev, Proc. CFC's: The Day After, IIR Comm B1, B2, E1, E2, 1994, p. 21.
Grigiante, M., G. Scalabrin, G. Benedetto, R. M. Gavioso, and R. Spagnolo, Fluid Phase Equilib. **174**, 69 (2000).
Gunther, D. and F. Steimle, Int. J. Refrig. **20**, 235 (1997).
Higashi, Y., Int. J. Refrig. **17**, 524 (1994).
Holian, K. S., *T-1 Handbook of Material Properties Data Bases*, Vol. Ic: *Equations of State* (Los Alamos National Laboratory, 1984), Report No. LA-10160-MS.
Hozumi, T., H. Sato, and K. Watanabe, Int. J. Thermophys. **17**, 587 (1996).
Ichikawa, T., K. Ogawa, H. Sato, and K. Watanabe, Speed-of-Sound Measurements for Gaseous Pentafluoroethane and Binary Mixture of Pentafluoroethane+1,1,1-Trifluoroethane, Department of System Design Engineering, Faculty of Science and Technology, Keio University, Yokohama, Japan, 1998.
Jacobsen, R. T, S. G. Penoncello, and E. W. Lemmon, Fluid Phase Equilib. **80**, 45 (1992).
Kamei, A., S. W. Beyerlein, and R. T Jacobsen, Int. J. Thermophys. **16**, 1155 (1995).
Kan, T., G. Yasuda, M. Suzuki, H. Sato, and K. Watanabe, Proc. 33rd National Heat Transfer Symposium of Japan, Nigata, Japan, 1996, p. 169.
Katti, R. S., R. T Jacobsen, R. B. Stewart, and M. Jahangiri, Adv. Cryo. Eng. **31**, 1189 (1986).
Kraft, K. and A. Leipertz, Int. J. Thermophys. **15**, 387 (1994).
Kuwabara, S., H. Aoyama, H. Sato, and K. Watanabe, J. Chem. Eng. Data **40**, 112 (1995).
Lee, B.-G., J.-Y. Park, J. S. Lim, and Y.-W. Lee, J. Chem. Eng. Data **45**, 760 (2000).
Lemmon, E. W. and R. T Jacobsen, J. Phys. Chem. Ref. Data **29**, 521 (2000).
Lemmon, E. W., R. T Jacobsen, S. G. Penoncello, and D. G. Friend, J. Phys. Chem. Ref. Data **29**, 331 (2000).
Lüddecke, T. O. and J. W. Magee, Int. J. Thermophys. **17**, 823 (1996).
Magee, J. W., Int. J. Thermophys. **17**, 803 (1996).
Marx, V., A. Pruß, and W. Wagner, Fortschr.-Ber. VDI, Dusseldorf: VDI-Verlag **19**(57) (1992).
McCarty, R. D. and V. D. Arp, Adv. Cryo. Eng. **35**, 1465 (1990).
Miyamoto, H. and K. Watanabe, Int. J. Thermophys. **21**, 1045 (2000).
Mohr, P. J. and B. N. Taylor, J. Phys. Chem. Ref. Data **28**, 1713 (1999).
Monluc, Y., T. Sagawa, H. Sato, and K. Watanabe, Proc. 12th Japan Symp. Thermophys. Prop., 1991, p. 65.
Nagel, M. and K. Bier, DKV-Tagungsbericht **20**, 39 (1993).
Oguchi, K., A. Murano, K. Omata, and N. Yada, Int. J. Thermophys. **17**, 55 (1996).
Outcalt, S. L. and M. O. McLinden, Int. J. Thermophys. **16**, 79 (1995).
Outcalt, S. L. and M. O. McLinden, J. Phys. Chem. Ref. Data **25**, 605 (1996).
Penoncello, S. G., A. R. H. Goodwin, and R. T Jacobsen, Int. J. Thermophys. **16**, 519 (1995).
Penoncello, S. G., E. W. Lemmon, R. T Jacobsen, and Z. Shan, J. Phys. Chem. Ref. Data **32**, 1473 (2003).
Perkins, R. A., NIST, 325 Broadway, Boulder, Colorado (private communication, 2002).
Piao, C.-C. and M. Noguchi, J. Phys. Chem. Ref. Data **27**, 775 (1998).
Preston-Thomas, H., Metrologia **27**, 3 (1990).
Sagawa, T., M. S. Thesis, Keio University, 1994.
Sagawa, T., H. Sato, and K. Watanabe, High Temp.-High Press. **26**, 193 (1994).
Schmidt, J. W. and M. R. Moldover, J. Chem. Eng. Data **39**, 39 (1994).
Schmidt, R. and W. Wagner, Fluid Phase Equilib. **19**, 175 (1985).
Setzmann, U. and W. Wagner, J. Phys. Chem. Ref. Data **20**, 1061 (1991).
Singh, R. R., E. A. E. Lund, and I. R. Shankland, Proc. CFC and Halon International Conference, 1991, p. 451.
Smukala, J., R. Span, and W. Wagner, J. Phys. Chem. Ref. Data **29**, 1053 (2000).
Span, R., *Multiparameter Equations of State—An Accurate Source of Thermodynamic Property Data* (Springer, Berlin, 2000).
Span, R., E. W. Lemmon, R. T Jacobsen, W. Wagner, and A. Yokozeki, J. Phys. Chem. Ref. Data **29**, 1361 (2000).
Span, R. and W. Wagner, J. Phys. Chem. Ref. Data **25**, 1509 (1996).
Span, R. and W. Wagner, Int. J. Thermophys. **18**, 1415 (1997).
Sunaga, H., R. Tillner-Roth, H. Sato, and K. Watanabe, Int. J. Thermophys. **19**, 1623 (1998).
Takagi, T., J. Chem. Eng. Data **41**, 1325 (1996).
Takahashi, M., N. Shibasaki-Kitakawa, and C. Yokoyama, Int. J. Thermophys. **20**, 445 (1999).
Tegeler, Ch., R. Span, and W. Wagner, J. Phys. Chem. Ref. Data **28**, 779 (1999).
Tillner-Roth, R., *Fundamental Equations of State* (Shaker Verlag, Aachen, Germany, 1998).
Tillner-Roth, R. and A. Yokozeki, J. Phys. Chem. Ref. Data **25**, 1273 (1997).
Tillner-Roth, R. and H. D. Baehr, J. Phys. Chem. Ref. Data **23**, 657 (1994).
Tillner-Roth, R., F. Harms-Watzenberg, and H. D. Baehr, DKV-Tagungsbericht **20**, 167 (1993).
Tsvetkov, O. B., A. V. Kletski, Yu. A. Laptev, A. J. Asambaev, and I. A. Zausaev, Int. J. Thermophys. **16**, 1185 (1995).
Wagner, W. and A. Pruß, J. Phys. Chem. Ref. Data **31**, 387 (2002).
Wagner, W., *Fortschr.-Ber. VDI* (VDI-Verlag, Dusseldorf, 1974), p. 3.
Weber, L. A. and A. M. Silva, J. Chem. Eng. Data **39**, 808 (1994).
Widiatmo, J. V., H. Sato, and K. Watanabe, J. Chem. Eng. Data **39**, 304 (1994).
Wilson, L. C., W. V. Wilding, G. M. Wilson, R. L. Rowley, V. M. Felix, and T. Chisolm-Carter, Fluid Phase Equilib. **80**, 167 (1992).
Ye, F., H. Sato, and K. Watanabe, J. Chem. Eng. Data **40**, 148 (1995).
Yokozeki, A., H. Sato, and K. Watanabe, Int. J. Thermophys. **19**, 89 (1998).
Younglove, B. A. and M. O. McLinden, J. Phys. Chem. Ref. Data **23**, 731 (1994).
Younglove, B. A., J. Phys. Chem. Ref. Data **11** (1982).
Zhang, H.-L., H. Sato, and K. Watanabe, J. Chem. Eng. Data **41**, 1401 (1996).
Zhang, H.-L., H. Sato, and K. Watanabe, Proc. 19th Int. Congress Refrig., The Hague, The Netherlands, Vol. IVA, 1995, p. 622.